

## Central Lancashire Online Knowledge (CLoK)

Title	Ionic Liquids on Oxide Surfaces
Type	Article
URL	<a href="https://clock.uclan.ac.uk/40952/">https://clock.uclan.ac.uk/40952/</a>
DOI	<a href="https://doi.org/10.1088/1361-648X/ac5994">https://doi.org/10.1088/1361-648X/ac5994</a>
Date	2022
Citation	Cole, Jordan and Syres, Karen orcid iconORCID: 0000-0001-7439-475X (2022) Ionic Liquids on Oxide Surfaces. Journal of Physics: Condensed Matter, 34 (21). ISSN 0953-8984
Creators	Cole, Jordan and Syres, Karen

It is advisable to refer to the publisher's version if you intend to cite from the work.  
<https://doi.org/10.1088/1361-648X/ac5994>

For information about Research at UCLan please go to <http://www.uclan.ac.uk/research/>

All outputs in CLoK are protected by Intellectual Property Rights law, including Copyright law. Copyright, IPR and Moral Rights for the works on this site are retained by the individual authors and/or other copyright owners. Terms and conditions for use of this material are defined in the <http://clock.uclan.ac.uk/policies/>

TOPICAL REVIEW • OPEN ACCESS

## Ionic liquids on oxide surfaces

To cite this article: Jordan Cole and Karen L Syres 2022 *J. Phys.: Condens. Matter* **34** 213002

View the [article online](#) for updates and enhancements.

You may also like

- [Simulations and Experiments of the Kinetics of the Electrochemical Double Layer in Ionic Liquids](#)  
Can Berk Uzundal, Pinar Aydogan-Gokturk, Sefik Suzer et al.
- [A Study on Rate Capacity and Safety of Ionic Liquid-Based Lithium Ion Battery](#)  
Takuya Nishimura and Katsunori Kojima
- [Mixtures of Ionic Liquid and Organic Electrolyte with Improved Safety and Electrochemical Performance with Nanostructured Silicon-Anode for Li-Ion Batteries](#)  
Gaiid P. Pandey, Lamartine Meda and Jun Li



**IOP | ebooks™**

Bringing together innovative digital publishing with leading authors from the global scientific community.

Start exploring the collection—download the first chapter of every title for free.

## Topical Review

# Ionic liquids on oxide surfaces

Jordan Cole<sup>ID</sup> and Karen L Syres\*<sup>ID</sup>

Jeremiah Horrocks Institute for Mathematics, Physics and Astronomy, University of Central Lancashire, Preston, PR1 2HE, United Kingdom

E-mail: [JCole4@uclan.ac.uk](mailto:JCole4@uclan.ac.uk) and [KSyres@uclan.ac.uk](mailto:KSyres@uclan.ac.uk)

Received 22 December 2021, revised 11 February 2022

Accepted for publication 1 March 2022

Published 25 March 2022

**Abstract**

Ionic liquids (ILs) supported on oxide surfaces are being investigated for numerous applications including catalysis, batteries, capacitors, transistors, lubricants, solar cells, corrosion inhibitors, nanoparticle synthesis and biomedical applications. The study of ILs with oxide surfaces presents challenges both experimentally and computationally. The interaction between ILs and oxide surfaces can be rather complex, with defects in the oxide surface playing a key role in the adsorption behaviour and resulting electronic properties. The choice of the cation/anion pair is also important and can influence molecular ordering and electronic properties at the interface. These controllable interfacial behaviours make ionic liquid/oxide systems desirable for a number of different technological applications as well as being utilised for nanoparticle synthesis. This topical review aims to bring together recent experimental and theoretical work on the interaction of ILs with oxide surfaces, including TiO<sub>2</sub>, ZnO, Al<sub>2</sub>O<sub>3</sub>, SnO<sub>2</sub> and transition metal oxides. It focusses on the behaviour of ILs at model single crystal surfaces, the interaction between ILs and nanoparticulate oxides, and their performance in prototype devices.

Keywords: ionic liquids, oxides, surfaces, interfaces, nanoparticle synthesis, TiO<sub>2</sub>, ZnO

(Some figures may appear in colour only in the online journal)

**1. Introduction**

The unique properties of ionic liquids (ILs) show great potential for transforming industrial processes, including CO<sub>2</sub> absorption [1, 2], catalysis [3, 4], batteries [5, 6], lubrication [7, 8] and photovoltaic devices [9, 10]. ILs are salts, composed solely of anions and cations, held together by their Coulomb potential. Unlike inorganic salts, such as NaCl, they tend to be liquid at room temperature due to their large, asymmetric ions which do not pack easily into crystals. There are millions of possible combinations of ions and these can be tuned to achieve desired properties. Figure 1 and table 1 show a selection of common cations and anions that have been studied

extensively in the literature. ILs have ultra-low vapour pressures, are non-flammable, have excellent thermal stability, a wide liquid range and a wide electrochemical window, which makes them very useful in a variety of potential applications. Optimising ILs for these different technologies relies on understanding chemical, structural, mechanical and charge transfer processes at interfaces.

ILs have been studied at the IL/vacuum (or IL/air) interface using a variety of techniques [11, 12]. For imidazolium-based ILs, the surface of the liquid contains the alkyl chains of the imidazolium ion facing outwards towards the vacuum (or air) in an ordered fashion, with a charged underlayer just beneath containing the anion and the charged part of the imidazolium cation. There have been many studies at the IL/metal interface [13–17]. Studies have shown that the structure the IL forms on the surface is coverage dependent, for example, one study found an IL formed a bilayer structure at sub-monolayer coverage but a checkerboard arrangement at higher coverage [18].

\* Author to whom any correspondence should be addressed.

 Original content from this work may be used under the terms of the [Creative Commons Attribution 4.0 licence](https://creativecommons.org/licenses/by/4.0/). Any further distribution of this work must maintain attribution to the author(s) and the title of the work, journal citation and DOI.

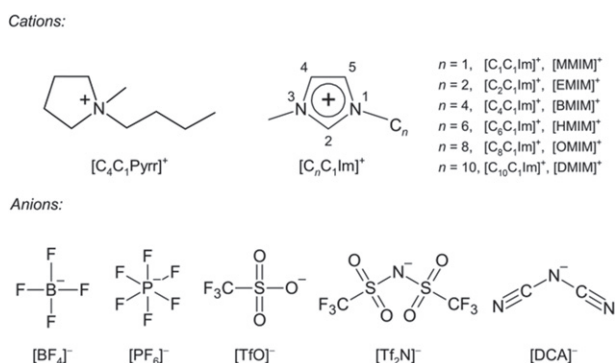


**Figure 1.** Structure of common IL cations and anions discussed in this review.

It has been found that the interaction between an IL and a channelled metal surface can cause ordering of the IL as well as changing the reconstruction adopted by the metal surface [16]. Studies have also identified the formation of IL islands or droplets on metal surfaces [15, 19, 20].

In comparison, studies of ILs at oxide surfaces are sparser. Experimentally, oxide surfaces can be challenging to prepare, particularly in the preparation of model single crystal surfaces or thin oxide films for surface science experiments. Single crystal metal oxide surfaces are usually prepared in ultra-high vacuum by sputter/anneal cycles.  $\text{Ar}^+$  ions are accelerated into the sample which sputters off the top layer of material and removes surface contamination with it. Subsequent annealing is required, sometimes in the presence of oxygen, to restore the surface crystallography and to remove embedded Ar atoms. Several sputter/anneal cycles are required to prepare a well-ordered atomically clean surface. Even then, the surface will have lattice defects, such as oxygen vacancies and step edges. Defects often determine the electronic and optical properties of the material and provide potential bonding sites for adsorbed atoms and molecules. In turn, the adsorption of molecules on the surface can shift the electronic bands in the oxide material. The interaction of molecules with oxide surfaces is therefore rather complex. Several theoretical models have been developed to model the properties of oxide surfaces and their interaction with adsorbates [21]. These provide interesting stand-alone results and aid in the interpretation of experimental data. Widely studied oxide substrates include  $\text{TiO}_2$ ,  $\text{ZnO}$ ,  $\text{SnO}_2$ ,  $\text{CeO}_2$ ,  $\text{Al}_2\text{O}_3$ ,  $\text{Fe}_2\text{O}_3$ ,  $\text{CuO}$ ,  $\text{MgO}$  and  $\text{NiO}$  due to their use in numerous technological and medical applications. More specifically for IL adsorbates, there are only a handful of studies at model single crystal oxide surfaces, which are detailed in this review. There are a greater number of studies on the interaction of ILs with nanoparticulate oxide surfaces, since many of their potential applications use oxides in nanoparticulate form. A good understanding of how ILs behave at these interfaces is vital since it underpins how the materials will perform in devices and other applications.

One widely studied potential application of ILs is as electrolytes in batteries, capacitors and other electrochemical applications. ILs can be used directly as electrolytes in many electrochemical systems due to their ionic conductivity. In some systems, ILs can be used as a one-component electrolyte

rather than a three-component electrolyte, which involve a solvent, supporting electrolyte and electroactive species. Electrochemistry in ILs is much more complicated than conventional electrochemistry [6]. The process of diffusion towards the electrode in IL electrolytes is somewhere between that of conventional electrolytes and solid-state diffusion. This is because ILs are generally viscous and have large asymmetrical ions and this can affect the diffusion pathway. In some electrochemical applications, ILs are mixed with conventional electrolytes. The combination can improve properties such as viscosity and conductivity. Liquid electrolytes are a safety concern in batteries because of possible leakage, so there have been studies into creating gel-polymer electrolytes, which also utilise ILs. The electrodes in these electrochemical devices are in direct contact with the IL electrolyte. Depending on the application, electrodes might be made from carbon, metal or metal oxide materials.

Over recent years, ILs have been incorporated into photovoltaic devices, including dye-sensitised solar cells (DSSCs) and perovskite solar cells. DSSCs were first proposed by Grätzel in 1991 as a cheaper alternative to silicon solar cells [22]. The design (shown schematically in figure 2) has since been developed and commercialised. DSSCs contain a dye which absorbs the incoming light. When the dye absorbs a photon, an electron in the dye is excited to a higher state and subsequently injected into the conduction band of a semiconductor, usually  $\text{TiO}_2$ . These electrons drift through the porous  $\text{TiO}_2$  to an electrode. The electron lost from the dye is replaced by another electron, usually from the valence band of a liquid electrolyte (typically the redox pair  $\text{I}^-/\text{I}_3^-$ ) or a solid state hole conductor (such as p-type semiconductors or polymers). This in turn is in contact with the counter electrode and the circuit is completed. The regeneration process of the dye is shown in figure 2(b) [23]. ILs have been incorporated into DSSCs as electrolytes to improve the stability of the devices. Perovskite-structured compounds were first used as light harvesters in solar cells in 2012 and have seen rapid increases in efficiencies to over 25% [24, 25]. Their major obstacle is their long-term instability, particularly under UV light and in the presence of water vapour, and this must be overcome before they can be commercialised. Similarly to DSSCs, perovskite solar cells consist of an electron-transport layer (ETL), usually  $\text{TiO}_2$  or  $\text{ZnO}$ , between the perovskite and electrode which helps with charge carrier separation. However, the electrons are often not transported efficiently and tend to recombine in the perovskite or become trapped in the ETL. ILs have been incorporated into these devices to aid with charge transport and stability issues.

ILs are used in a process called solid catalyst with ionic liquid layer (SCILL) which uses a solid heterogeneous catalyst coated with a thin layer of IL to ‘tune’ the selectivity of the catalyst [26]. They are also used in supported ionic liquid phase (SILP) catalysis, where a thin layer of IL containing the catalyst is spread over a high-surface-area support. For SCILL and SILP catalysis, the IL is dispersed on a high-surface-area oxide support, for example alumina or silica. Studies of the behaviour at the interface of the IL and oxide support material are important to determine how the IL adheres

**Table 1.** Names and acronyms of common IL cations and anions discussed in this review.

Acronym	Name
<b>Cations</b>	
[C <sub>1</sub> C <sub>1</sub> Im]/[MMIM]	1,3-dimethylimidazolium
[C <sub>2</sub> C <sub>1</sub> Im]/[EMIM]	1-ethyl-3-methylimidazolium
[C <sub>3</sub> C <sub>1</sub> Im]/[PMIM]	1-propyl-3-methylimidazolium
[C <sub>4</sub> C <sub>1</sub> Im]/[BMIM]	1-butyl-3-methylimidazolium
[C <sub>6</sub> C <sub>1</sub> Im]/[HMIM]	1-hexyl-3-methylimidazolium
[C <sub>10</sub> C <sub>1</sub> Im]/[DMIM]	1-decyl-3-methylimidazolium
[C <sub>2</sub> C <sub>2</sub> Im]/[EEIM]	1,3-diethylimidazolium
[C <sub>4</sub> C <sub>1</sub> Pyrr]/[BMP]	1-butyl-1-methylpyrrolidinium
[DEME]	N,N-diethyl-N-(2-methoxyethyl)-N-methylammonium
<b>Anions</b>	
[BF <sub>4</sub> ]	Tetrafluoroborate
[PF <sub>6</sub> ]	hexafluorophosphate
[NO <sub>3</sub> ]	Nitrate
[Cl]	Chloride
[I]	Iodide
[TfO]	Trifluoromethanesulfonate
[Tf <sub>2</sub> N]	Bis(trifluoromethanesulfonyl)imide
[MeSO <sub>4</sub> ]	Methylsulfate
[DCA]	Dicyanamide
[SCN]	Thiocyanate
[TBC]	Tetracyanoborate

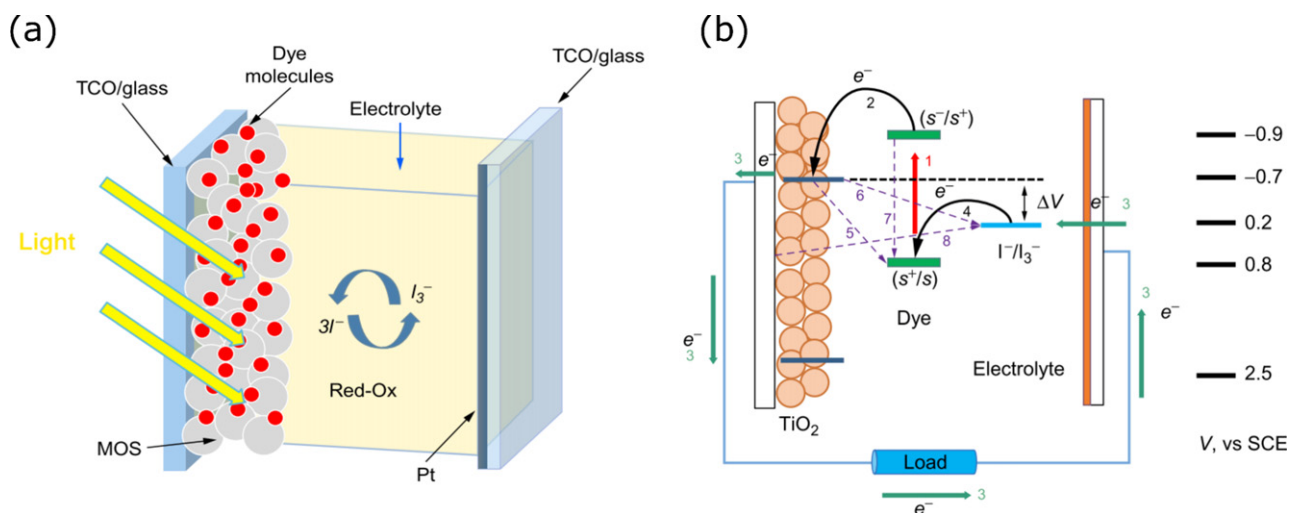


**Figure 2.** (a) Schematic of a DSSC and (b) process for dye regeneration. Reprinted from [23], Copyright (2018), with permission from Elsevier.

and disperses on the support and the chemical properties at the interface [26].

The IL/solid interface is also the subject of many tribology studies, with steel, Fe, Al and Cu being common metal substrates and SiO<sub>2</sub> a common oxide substrate [27]. In the field of tribology, ILs are being investigated as lubricants, particularly for extreme conditions where other liquid lubricants fail. Due to increasing loads and smaller components, thinner lubricating films are becoming necessary. ILs can adsorb onto a metal surface and produce a thin, protective film. Under high

pressure, some ILs react to form a protective tribofilm, particularly with ILs containing fluorine, phosphorus or boron [7].

ILs can also be used in a different capacity; to synthesise nanoparticles. ILs have been used as solvents, reactants or templates in the synthesis of nanomaterials [28]. ILs have many advantages in synthetic procedures. They have low interface tensions which results in high nucleation rates of the product. The IL can also interact with the products, for example, via hydrogen bonding, which can affect the shape of the prod-

ucts. ILs have been used to make a variety of metal and oxide nanoparticles with controllable morphologies and properties [28].

In this review, we will discuss the most widely studied oxide surfaces. We will focus on key results from studies of ILs at model single crystal oxide surfaces, studies of ILs with oxide nanoparticles and a summary of how IL/oxide systems have been incorporated into prototype devices and other applications.

## 2. Ionic liquids on $\text{TiO}_2$ surfaces

$\text{TiO}_2$  surfaces have been a popular choice of substrate in the study of ILs at oxide surfaces. Many technological applications consist of nanoparticulate  $\text{TiO}_2$ . The anatase  $\text{TiO}_2$  (101) surface is thought to be the dominant surface in  $\text{TiO}_2$  nanoparticles because it has the lowest surface energy [29]. The rutile  $\text{TiO}_2$  (110) surface in its  $(1 \times 1)$  termination is considered as a model metal oxide surface for surface science studies. The unit cell structure of anatase and rutile  $\text{TiO}_2$  are shown in figure 3, as well as another common polymorph, brookite. In this section, we will review studies of ILs on single crystal surfaces, studies of ILs on nanoparticulate or thin films of  $\text{TiO}_2$ , and the performance of ILs/ $\text{TiO}_2$  in prototype devices.

### 2.1. Ionic liquids on single crystal $\text{TiO}_2$ surfaces

**2.1.1. Anatase  $\text{TiO}_2$  (101).** Weber *et al* developed computational methods to study a variety of ILs on the anatase  $\text{TiO}_2$  (101) surface [31–33]. They studied the adsorption behaviour of the ILs  $[\text{C}_1\text{C}_1\text{Im}][\text{SCN}]$  and  $[\text{C}_1\text{C}_1\text{Im}][\text{TBC}]$  [32]. They discovered that the surface titanium atoms are predominantly in contact with the nitrogen atoms of the anion. The surface oxygen atoms interact via hydrogen-bond-like structures with the hydrogen atoms in the imidazolium cation, as well as electrostatic and dispersive interactions. They found that the ion pairs remain stable following adsorption on the surface and their geometry remains similar to that of the isolated ions. Their results show that the adsorption of the IL caused a band shift of the density of states of  $\text{TiO}_2$ . The authors carried out a further investigation of a variety of ILs on the anatase  $\text{TiO}_2$  (101) surface, specifically looking for changes in band energy levels of the  $\text{TiO}_2$  [33]. They found that in general, the cations caused a downward shift of the  $\text{TiO}_2$  energy levels and the anions caused an upwards shift of the energy levels, by accepting/donating electron density from/to the surface, respectively. The final outcome therefore depends on the combination of the cation and anion. From the ILs they studied, they found that  $[\text{C}_2\text{C}_2\text{Im}][\text{Cl}]$  gave the highest energetic upward shift and  $[\text{C}_2\text{C}_1\text{Im}][\text{PF}_6]$  gave the largest energetic downward shift. Overall, the different anions studied gave a larger range of energetic shifts compared to the minimal effect of changing the cation.

Photoemission and x-ray absorption techniques have been used to experimentally examine the anatase/IL interface. Wagstaffe *et al* used x-ray photoelectron spectroscopy (XPS)

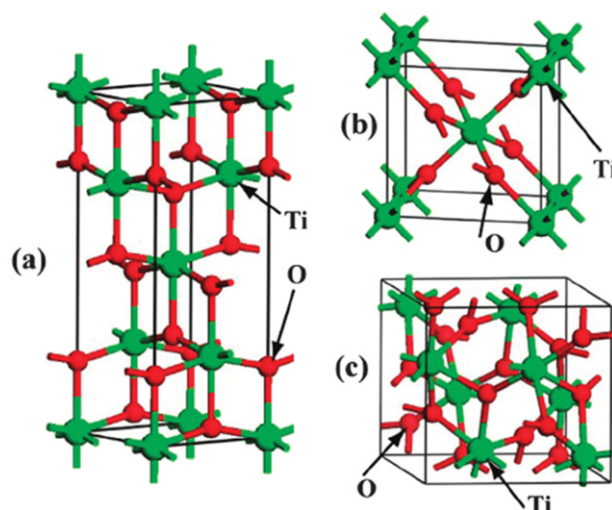


**Figure 3.** Schematic unit cells for (a) anatase, (b) rutile and (c) brookite  $\text{TiO}_2$ . The large green spheres represent Ti atoms and the small red spheres represent O atoms. Reproduced from [30] with permission from the Royal Society of Chemistry.

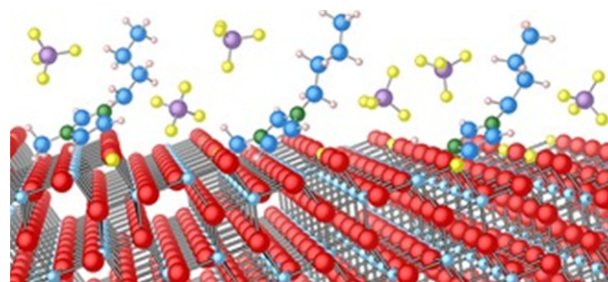


**Figure 4.** Schematic representation of the interaction of  $[\text{C}_4\text{C}_1\text{Im}][\text{BF}_4]$  with the anatase  $\text{TiO}_2$  (101) surface. Reproduced from [34]. CC BY 4.0.

and near-edge x-ray absorption fine structure (NEXAFS) spectroscopy to study the interaction of  $[\text{C}_4\text{C}_1\text{Im}][\text{BF}_4]$  with a single crystal anatase  $\text{TiO}_2$  (101) surface [34]. At low coverages, they found the IL orders on the surface via electrostatic attraction, with the imidazolium ring oriented at about  $32^\circ \pm 4^\circ$  from the surface as shown in figure 4. As they increased the coverage, they found the ordering of the IL was lost, as the IL layers become less influenced by the presence of the surface.

**2.1.2. Rutile  $\text{TiO}_2$  (110).** The interaction of ILs with the rutile  $\text{TiO}_2$  (110) surface has been studied using a variety of computational and experimental techniques. Molecular dynamics simulations of  $[\text{C}_4\text{C}_1\text{Im}][\text{NO}_3]$  on the  $\text{TiO}_2$  (110) surface reveal that  $[\text{NO}_3]^-$  anions segregate and bind to the  $\text{TiO}_2$  surface in a highly ordered manner [35]. The  $[\text{C}_4\text{C}_1\text{Im}]$  cations occupy the next layer and their orientation is modulated by the layer of adsorbed anions. The imidazolium ring of the  $[\text{C}_4\text{C}_1\text{Im}]$  cation stands vertically, almost perpendicular to the  $\text{TiO}_2$  surface (see figure 5). Malali and Foroutan used molecular dynamics simulations to study the wetting behaviour of  $[\text{C}_4\text{C}_1\text{Im}][\text{PF}_6]$  on the  $\text{TiO}_2$  (110) surface [36]. Here they

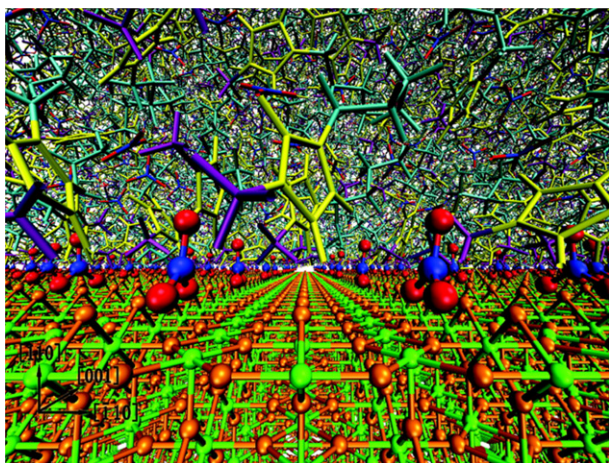


**Figure 5.** A snapshot taken from a molecular dynamics simulation at the IL/rutile (110) interfacial region: green, Ti-atom; orange, O-atom of  $\text{TiO}_2$ ; blue, N-atom of  $[\text{NO}_3]^-$ ; red, O-atom of  $[\text{NO}_3]^-$ ; yellow, imidazolium ring; purple, methyl group; cyan, butyl group. Reprinted with permission from [35]. Copyright (2007) American Chemical Society.

found that a  $[\text{C}_4\text{C}_1\text{Im}]$  cation-rich layer is spread on the surface, with the imidazolium rings parallel to the  $\text{TiO}_2$  surface, however, the orientation of the rings in the upper layer of the drop is almost vertical. They found the interaction between the substrate and IL leads to a circular configuration of ions in the centre of the droplet. This results in wetting behaviour of the IL in the adjacent layer to the surface but nonwetting behaviour at long distances from the surface.

*In situ* XPS was employed by Henderson *et al* to study a thin layer of  $[\text{C}_4\text{C}_1\text{Im}][\text{BF}_4]$  on the rutile surface when exposed to water vapour [37]. They observed a reordering of the IL as water adsorbed to the IL layers. ILs are prone to absorb water and it is likely to be present in many of their potential applications. The same group studied a thin film of the superbasic IL trihexyltetradecylphosphonium benzimidazolide ( $[\text{P}_{66614}][\text{benzim}]$ ) on rutile  $\text{TiO}_2$  (110) and exposed it to  $\text{CO}_2$  at near-ambient pressures. They combined *in situ* XPS and NEXAFS measurements with density functional theory (DFT) simulations and found a realignment of the  $[\text{benzim}]^-$  anions from  $27^\circ$  from the surface normal to  $54^\circ$  upon exposure to  $\text{CO}_2$  [38]. These studies highlight the importance of water and other gases in the study of IL/ $\text{TiO}_2$  systems and the implications for IL thin film catalysis and gas capture applications.

XPS has also been used alongside scanning tunnelling microscopy (STM) to investigate the interaction of  $[\text{C}_4\text{C}_1\text{Pyrr}][\text{Tf}_2\text{N}]$  with a reduced rutile  $\text{TiO}_2$  (110) ( $1 \times 1$ ) surface [39]. At lower temperatures STM images reveal  $[\text{C}_4\text{C}_1\text{Pyrr}][\text{Tf}_2\text{N}]$  adsorbed molecularly on the surface with even coverage in lines along the [001] direction. However, at higher temperatures above 380 K, decomposition occurs. Degradation mechanisms of the  $[\text{Tf}_2\text{N}]^-$  anion and  $[\text{C}_4\text{C}_1\text{Pyrr}]^+$  cation are shown in figure 6 [39–42]. Decomposition products included  $\text{S}_{\text{ad}}$ ,  $\text{F}_{\text{ad}}$  and  $\text{TiN}_x$ . The IL was found to decompose at lower temperatures ( $\sim 300$  K) when the  $\text{TiO}_2$  surface was pre-covered with Li. This was

due to the formation of  $\text{Ti}^{3+}$  and  $\text{Li}^+$  species intercalated at the near-surface region. Degradation of the IL at these temperatures has implications for the operating temperatures of IL-based Li-ion batteries.

Suzuki *et al* used transmission electron spectroscopy (TEM) and atomic force microscopy (AFM) to study the adsorption of Au nanoparticles encapsulated in ILs on the rutile  $\text{TiO}_2$  (110) surface [43]. Their results suggest that the chemical nature of the IL affects the immobilisation of the Au nanoparticles through hydrogen bonding or coordination bonding with the surface. They suggested that a layer of IL on the  $\text{TiO}_2$  surface might influence the size and surface density of nanoparticles and may show potential for controlling the location nanoparticles on the surface.

## 2.2. Ionic liquids on nanoparticulate $\text{TiO}_2$

### 2.2.1. Synthesis of $\text{TiO}_2$ nanostructures using ionic liquids.

A 2011 review by Liu *et al* provided an overview of how ILs have been employed for the preparation of inorganic nanomaterials, including  $\text{TiO}_2$  [28]. In this section, we will summarise some specific examples where ILs have been used to synthesise a variety of  $\text{TiO}_2$  nanostructures.

Nakashima and Kimizuka developed a single-step synthesis of hollow titania microspheres in ILs [44]. Imidazolium molecules in the IL act both as a solvent and a stabiliser for the hollow microspheres. Anatase  $\text{TiO}_2$  nanoparticles have been synthesised with uniform size and shape using a microwave-assisted method in  $[\text{C}_4\text{C}_1\text{Im}][\text{BF}_4]$  [45], while the similar IL  $[\text{C}_4\text{C}_1\text{Im}][\text{Cl}]$  has been used as a co-solvent to synthesise nanoporous rutile  $\text{TiO}_2$  with different morphologies via a simple one-pot method [46].

ILs are also effective electrolytes for producing  $\text{TiO}_2$  nanotube arrays such as those shown in figure 7 [47]. These can be grown electrochemically using titanium foil as an anode and  $[\text{C}_4\text{C}_1\text{Im}][\text{BF}_4]$  as an electrolyte [47, 48]. The high conductivity of the IL gives fast pore widening and few contaminants from electrolyte decomposition.

Mali *et al* used a hydrothermal method in a Brønsted acidic IL to synthesise rutile  $\text{TiO}_2$  nanoflowers comprising of bunches of aligned nanorods [49]. Shahi *et al* synthesised  $\text{TiO}_2$  nanostructures using an IL aqueous medium and found the formation of thin flaky  $\text{TiO}_2$  nanorods, which look like nanoflowers, by a sol–gel method but well-defined solid rutile nanorods with a hydrothermal method [50].

### 2.2.2. Interaction of $\text{TiO}_2$ nanoparticles with ILs.

There have been numerous studies of the interaction of nanoparticulate  $\text{TiO}_2$  with ILs using a variety of techniques. Since  $\text{TiO}_2$  is in nanoparticulate form in most of its potential applications, these studies aiming to understand the interfacial behaviour are very important. Chang *et al* used high-pressure infrared spectroscopy to probe the local structures between nano- $\text{TiO}_2$  and  $[\text{C}_2\text{C}_1\text{Im}][\text{TfO}]$  and  $[\text{C}_4\text{C}_1\text{Im}][\text{TfO}]$  [51]. They found that the high pressure enhanced imidazolium CH- $\text{TiO}_2$  interactions. Their study suggests that the alkyl chain length of the imidazolium cation is an important factor in IL/nano- $\text{TiO}_2$  interactions. Hydrophobicity of the IL has also been found to

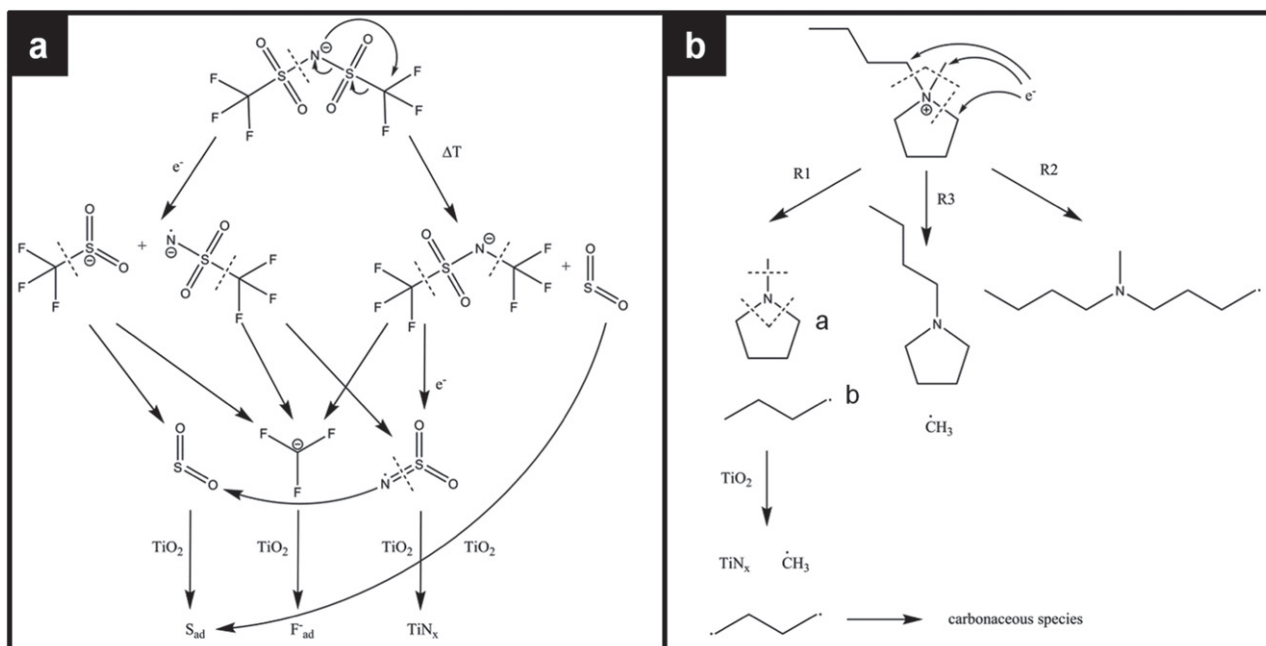


**Figure 6.** Possible decomposition mechanisms of (a) the  $[\text{Tf}_2\text{N}]^-$  anion and (b) the  $[\text{C}_4\text{C}_1\text{Pyr}]^+$  cation according to literature calculations [40–42] and thermal decomposition products found on the  $\text{TiO}_2$  (110) surface with XPS measurements. Reproduced from [39]. CC BY 3.0.

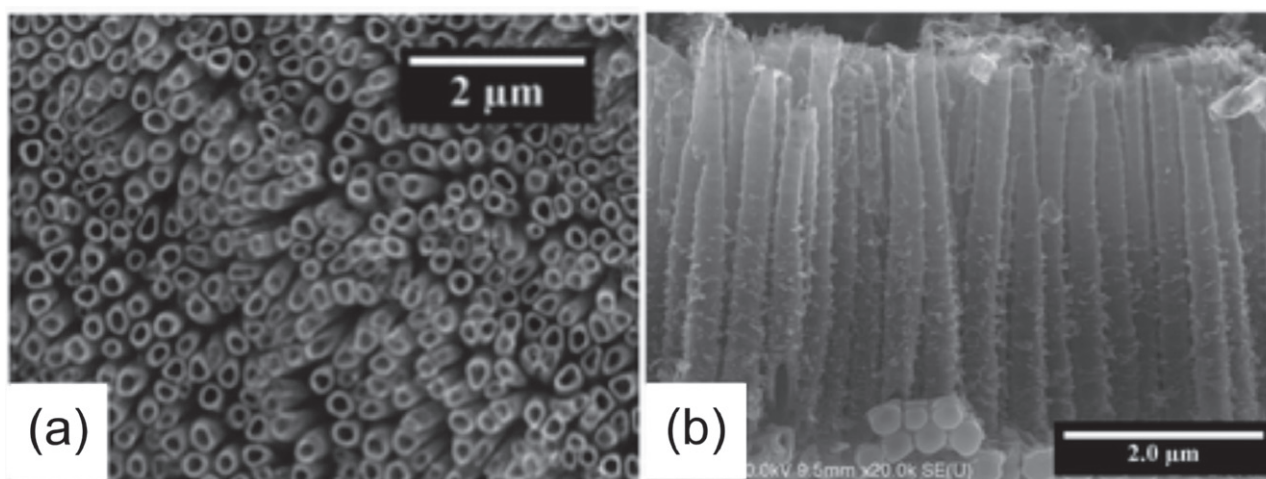


**Figure 7.** (a) Top morphology and (b) cross-section view of  $\text{TiO}_2$  nanotubes electrochemically grown in  $[\text{C}_4\text{C}_1\text{Im}][\text{BF}_4]$ -based electrolytes using a two-step anodisation procedure. Reproduced from [47] with permission from the Royal Society of Chemistry.

influence IL/ $\text{TiO}_2$  interactions. It has been shown that increasing the hydrophobicity of the IL increases the thickness of the IL film on nanoparticulate  $\text{TiO}_2$  surfaces [52].

Sum frequency generation vibrational spectroscopy and contact angle measurements were carried out by Aliaga and Baldelli to study the interfacial structure of the ILs  $[\text{C}_4\text{C}_1\text{Im}][\text{DCA}]$  and  $[\text{C}_4\text{C}_1\text{Im}][\text{MeSO}_4]$  on a  $\text{TiO}_2$  nanoparticle-coated  $\text{CaF}_2$  window [53]. Both ionic species were detected at the interface for  $[\text{C}_4\text{C}_1\text{Im}][\text{DCA}]$  but only the cation was detected for  $[\text{C}_4\text{C}_1\text{Im}][\text{MeSO}_4]$ . Their results suggest that the imidazolium ring of the ILs lies nearly parallel to the  $\text{TiO}_2$  surface.

An *et al* studied the wetting behaviour of  $[\text{C}_4\text{C}_1\text{Im}][\text{PF}_6]$  on mesoporous and dense  $\text{TiO}_2$  films using AFM [54]. They found it formed a wetting phase on mesoporous  $\text{TiO}_2$  films, but nonwetting and sphere-shaped droplets on dense films. On mesoporous films, the adhesive force of the IL reaches 40 nN, but only 4 nN on dense films. The stronger adhesive force on mesoporous films makes a contact angle of  $5^\circ$  and this remains after five months. The stable spreading of the IL provides large wetting areas and short  $\text{CO}_2$  diffusion distance on the mesoporous surface, enabling much higher  $\text{CO}_2$  capture rates than on dense  $\text{TiO}_2$  films or pure ILs. Solvents with faster  $\text{CO}_2$  absorption rates are desirable for post-combustion carbon

capture because they require smaller liquid–gas contact areas [55]. This would allow smaller absorption columns to be used in CO<sub>2</sub> capture processes, therefore reducing capital costs.

Fabregat-Santiago *et al* used cyclic voltammetry and impedance spectroscopy to study the electrochemical behaviour of nanoporous TiO<sub>2</sub> in [C<sub>2</sub>C<sub>1</sub>Im][Tf<sub>2</sub>N] [56]. Their results followed the same trends as for other organic solvents and aqueous electrolytes, so the authors concluded that the use of ILs in TiO<sub>2</sub>-based devices is feasible. Binetti *et al* used time-resolved spectroscopic measurements to study charge transfer between TiO<sub>2</sub> nanorods and imidazolium-based ILs dispersed in a solvent [57]. Their measurements suggest there is a charge-transfer process from the photoexcited TiO<sub>2</sub> nanorods to the imidazolium rings of ILs. Understanding charge transfer processes is important for improving the design of devices that are based on nanostructured metal oxides and ILs such as solar cells and batteries.

**2.2.3. Confined ionic liquids in nanoporous TiO<sub>2</sub>.** There are many complex interactions between confined ILs and their surrounding pore walls. This has been explored in many experimental and computational studies for a range of surfaces, as summarised in previous review papers [58, 59]. Nanoconfined IL films are defined as interacting with more than one wall, for example, the walls of a nanopore, or between the surfaces of two interacting colloidal particles [59]. Nanoconfined ILs exhibit vastly different physicochemical properties compared to bulk ILs, making them desirable for a wide range of energy applications including lubrication [60], gas capture and separation [61], inogels for supported catalysts [62], and supercapacitors [58]. Most of these aforementioned studies use silica or mica surfaces and membranes, however, metal oxide nanostructures are also excellent candidates for IL confinement. Verma *et al* studied confinement of the IL [C<sub>2</sub>C<sub>1</sub>Im][EtSO<sub>4</sub>] (1-ethyl-3-methylimidazolium ethyl sulphate) in anatase TiO<sub>2</sub> nanopores [63]. TiO<sub>2</sub> nanopowder synthesised without the IL resulted in amorphous nanoparticles, while IL-assisted synthesis resulted in nanoparticles with an anatase structure and an increased surface area. They found an increase in the glass transition temperature of the confined IL, and FTIR measurement revealed a change in the C–H vibrations of the alkyl chain and ring of the [C<sub>2</sub>C<sub>1</sub>Im]<sup>+</sup> cation.

Molecular dynamics simulations can also be used to study the structure and dynamics of nanoconfined ILs. Singh *et al* carried out molecular dynamics simulations of [C<sub>2</sub>C<sub>1</sub>Im][Tf<sub>2</sub>N] confined inside a rutile (110) slit nanopore (see figure 8) [64]. They found that electrostatic and dispersion interactions are present between the IL and the rutile walls. They suggest that the strength of the interactions between the pore walls and the IL can significantly affect the structure and dynamics of the confined IL. They found that ions near the rutile walls had a liquid structure significantly different from the bulk IL structure, and that cations and anions adopted multiple orientations near the rutile walls. In contrast, the same ions near graphitic pore walls had a liquid structure that was similar to that of the bulk IL and parallel orientations were uniformly observed for the same ions near graphitic walls [65]. They found the dynamics of [C<sub>2</sub>C<sub>1</sub>Im][Tf<sub>2</sub>N] inside a

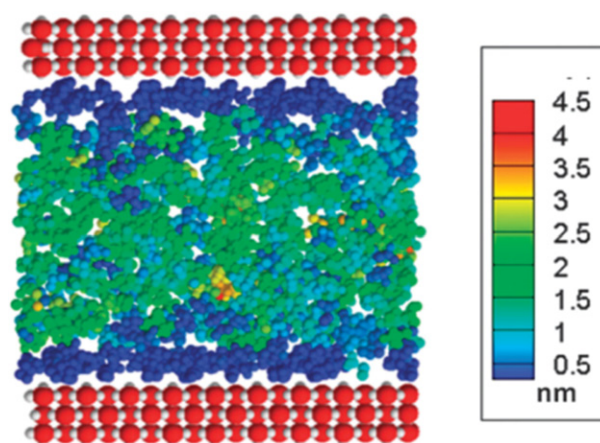


**Figure 8.** Total displacement of [Tf<sub>2</sub>N]<sup>−</sup> anions inside a rutile TiO<sub>2</sub> (110) slit pore over a time of 10 ns. Reproduced from [64] with permission from the Royal Society of Chemistry.

slit rutile pore to be significantly slower than those observed inside a slit graphitic pore. The group used the same method to study the structure and dynamics of a deep eutectic solvent, choline iodide-glycerol, inside the same rutile (110) slit nanopores [66] and their results were similar to those obtained for [C<sub>2</sub>C<sub>1</sub>Im][Tf<sub>2</sub>N].

### 2.3. Ionic liquids and TiO<sub>2</sub> in devices

Due to their thermal stability, high ionic conductivity and negligible vapour pressure, ILs are desirable as potential electrolytes in DSSCs. Studies have found that IL electrolytes could improve the stability of DSSCs. Papageorgiou *et al* found that ILs based on methyl-hexyl-imidazolium iodide had advantages over organic liquids as solvents for solar cell electrolytes and gave a cell performance with outstanding stability [67]. Other studies have used tetracyanoborate-based ILs [68, 69], as well as guanidinium thiocyanate [70, 71] and [C<sub>3</sub>C<sub>1</sub>Im][I] [72, 73] in DSSCs. IL electrolytes can be inkjet printed for use in a DSSC [74]. This new fabrication process eliminates drilling holes in the DSSC substrates. The technique reduces the fabrication cost and removes an additional step from the traditional cell sealing process.

Quasi-solid DSSCs can be fabricated by gelling IL electrolytes with phase-separated chemically cross-linked gels [75]. Kubo *et al* used [C<sub>6</sub>C<sub>1</sub>Im][I], iodine and a low molecular weight gelator as a quasi-solid-state electrolyte [76], whilst others used silica nanoparticles to solidify ILs [77]. Yamanaka *et al* fabricated a novel IL crystal system ([C<sub>12</sub>C<sub>1</sub>Im][I]/I<sub>2</sub>) with a smectic A phase as an electrolyte for a DSSC [78]. It showed a higher short-circuit current density and higher light-to-electricity conversion efficiency than the system using the non-liquid crystalline IL ([C<sub>11</sub>C<sub>1</sub>Im][I]/I<sub>2</sub>) due to the higher conductivity of the IL crystal. A quasi-solid-state IL crystal DSSC was also fabricated by using a low molecular gelator. Enhanced conductivity in the [C<sub>12</sub>C<sub>1</sub>Im][I]/I<sub>2</sub>–gel led to a higher light-to-electricity conversion efficiency and an increased short-circuit current density compared to [C<sub>12</sub>C<sub>1</sub>Im][I]/I<sub>2</sub> without gelator.

Bai *et al* optimised the lithium iodide content in  $[\text{C}_2\text{C}_1\text{Im}][\text{DCA}]$ -based IL electrolytes to produce a solvent-free DSSC with an 8.4% efficiency [79]. They reported a decrease in open-circuit photovoltage with the addition of lithium, as the titania conduction band edge shifts downwards, but this is partly compensated by a suppression of the triiodide involving interfacial charge recombination. Zhang *et al* investigated the effects of  $[\text{DCA}]^-$  versus  $[\text{TBC}]^-$  anions on the energetics of the titania conduction band edge and kinetics of multi-channel charge-transfer reactions in DSSCs [80]. They found that due to a more favourable thermodynamic driving force, the  $[\text{TBC}]^-$  anion prompts a much faster electron injection from the excited-state dye to titania than the  $[\text{DCA}]^-$  anion. They found that  $[\text{DCA}]^-$  at the titania/electrolyte interface reduced the electron exchange rate with triiodide, compared to  $[\text{TBC}]^-$ .

ILs have also been incorporated into perovskite solar cells. Perovskite solar cells consist of an ETL, such as  $\text{TiO}_2$ , between the perovskite and cathode which helps with charge carrier separation. However, the electrons have a tendency to recombine in the perovskite or become trapped in the ETL. It has been found that depositing a layer of IL at the interface between the perovskite and ETL [81], or mixing a small quantity of IL with the perovskite precursors [82, 83], results in more efficient electron transport and has been linked to an improvement in stability of the devices [84].

### 3. Ionic liquids on ZnO surfaces

ZnO is another popular oxide for studies of ILs and has been researched as an alternative to the widely studied  $\text{TiO}_2$  for a number of photovoltaic, photocatalytic, and optoelectronic applications. ZnO is an n-type semiconductor with a similar band gap (3.4 eV) to  $\text{TiO}_2$  (3.2 eV) and similar electron injection efficiencies [85, 86]. ZnO has a large exciton binding energy (60 meV) making it excellent for optoelectronic applications [87], while a higher electron mobility compared to  $\text{TiO}_2$  [88] makes ZnO a strong alternative in solar cell technologies. Anisotropic crystalline growth of ZnO facilitates increased dye anchoring in DSSCs [89, 90]. ZnO has a strong luminescence [91] and offers better photocatalytic degradation of organic compounds compared to  $\text{TiO}_2$  [92]. Unlike  $\text{TiO}_2$ , however, there are very few studies on the interaction between ILs and single crystal ZnO surfaces. Instead, there are many studies on the interactions of ILs with ZnO nanoparticles due to their wide range of uses and numerous synthesis methods. Here we will discuss common synthesis routes and applications of ZnO nanostructures using ILs. We will also explore the role of ILs as templates for tuning size, shape, and properties of ZnO nanostructures.

#### 3.1. Ionic liquids on nanostructured ZnO surfaces

Due to the quantum confinement effect [93], nanocrystalline metal oxides have many desirable size- and morphology-dependent properties such as band gap [94], photocatalytic activity [95], and photoluminescence [96]. Imidazolium-based

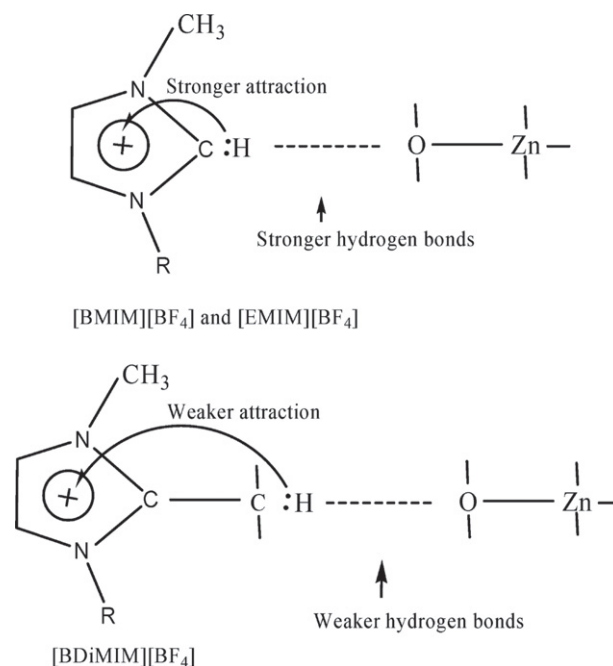


**Figure 9.** Schematic illustration of the comparison of hydrogen bonds between ZnO and the ILs [EMIM][ $\text{BF}_4$ ], [BMIM][ $\text{BF}_4$ ], and [BDiMIM][ $\text{BF}_4$ ] (1-*n*-butyl-2,3-dimethylimidazolium tetrafluoroborate). Reprinted with permission from [98]. Copyright (2008) American Chemical Society.

ILs serve as a green alternative to many volatile organic solvents commonly used in nanoparticle synthesis. They are also capable of generating highly-directional growth of primary nanoparticles due to strong hydrogen bonding between position 2 of the imidazolium ring (see figure 1) and O atoms in ZnO (figure 9) [97, 98]. There are also many quick and easy synthesis routes for ZnO nanoparticles and nanostructures using IL solvents, each offering a range of tunable morphologies. Changing the cation/anion pair of the IL, as well as synthesis conditions, enables control of crystallite size and uniformity [99], growth habit [100], optical properties [97], overall morphology, and more.

**3.1.1. Synthesis of ZnO nanostructures using ionic liquids.** It is common to synthesise nanomaterials using a microwave-assisted approach as it yields fast and simple nanostructure growth. ILs have been shown to be suitable solvents for microwave-assisted synthesis thanks to their desirable dielectric properties and negligible vapor pressure [101]. The IL serves as both a solvent for absorbing microwaves and as a template for tuning nanostructure morphology [102].  $[\text{C}_4\text{C}_1\text{Im}][\text{BF}_4]$  is a common solvent of choice to synthesise nanostructure ZnO. By controlling the concentration of  $[\text{C}_4\text{C}_1\text{Im}][\text{BF}_4]$  and the heating temperature, flower-like and needle-like morphologies can be achieved [103]. Wang *et al* compared the effect of changing the anion in  $[\text{C}_4\text{C}_1\text{Im}][\text{BF}_4]$  to  $[\text{Cl}]^-$  [104]. Microwave heating using  $[\text{C}_4\text{C}_1\text{Im}][\text{BF}_4]$  resulted in ZnO spheres with shuttle-like nanorods (irregular in morphology) growing on the sphere's surface. Meanwhile,  $[\text{C}_4\text{C}_1\text{Im}][\text{Cl}]$  yielded multipod structures comprised of homocentric nanorods approximately  $0.5 \mu\text{m}$  long. Further

heating increased the average length of nanorods to 1.5  $\mu\text{m}$  and resulted in flower-like structures. The absence of an IL resulted in no ZnO nanostructure formation, regardless of prolonged heating. This highlights the importance of the interplay between the IL and microwave heating in forming these ZnO nano-/microstructures.

Another common nanomaterial synthesis method is the sonochemical approach. High intensity ultrasound irradiation can cause acoustic cavitation, the rapid formation, growth and collapse of cavitating bubbles in a liquid [105]. This technique is capable of generating very high and localised temperatures and pressures in the liquid. These conditions can be exploited for nanoparticle synthesis, and the unique properties of ILs make them suitable solvents. Changing the IL in an IL-water mixture allows control of both particle size and overall morphology. This was confirmed with scanning electron microscope (SEM) imaging by Sabbaghan *et al* [99], revealing that cations with a shorter alkyl chain (1,4-diazabicyclo[2.2.2]octane) resulted in the formation of ZnO nanoparticles, non-uniform in both size and morphology. Increasing the alkyl chain length resulted in uniform 2D nanosheets while the use of a dicationic imidazolium based-IL resulted in nanoleaf morphology. Goharshadi *et al* used  $[\text{C}_6\text{C}_1\text{Im}][\text{Tf}_2\text{N}]$  as a solvent to obtain uniform nanocrystalline ZnO particles via the ultrasound-assisted decomposition of a zinc acetate precursor [106].

Ionothermal synthesis of nanomaterials is equivalent to hydrothermal synthesis with the exception that an IL is used as a solvent instead of water. Morris provides a detailed overview of this approach for a variety of materials in their review [107]. However, ionothermal synthesis of nanostructured metal oxides is less documented. Zhu *et al* used an ionothermal process with a metal-containing IL precursor to synthesise hierarchical ZnO structures with a range of morphologies [108]. The morphologies were found to be strongly controlled by the IL precursor. A hybrid solvothermal-ionothermal method performed by Zhang *et al* [109] demonstrated controllable synthesis of ZnO nanospheres by changing the length of the alkyl chain of imidazolium-based ILs:  $[\text{C}_2\text{C}_1\text{Im}][\text{BF}_4]$ ,  $[\text{C}_4\text{C}_1\text{Im}][\text{BF}_4]$  and  $[\text{C}_{10}\text{C}_1\text{Im}][\text{BF}_4]$ . Increasing the chain length did not change the type of nanostructure but increased the size of pore channels in hollow microspheres, leading to less well-defined morphologies.

Wang *et al* studied the effect of alkyl chain length in imidazolium-based ILs on the morphology of ZnO nanostructures using a low-temperature solid-state synthesis method [98]. They found that the longer alkyl chain in  $[\text{C}_4\text{C}_1\text{Im}][\text{BF}_4]$  limited the size of ZnO nanorods (200–600 nm) compared to  $[\text{C}_2\text{C}_1\text{Im}][\text{BF}_4]$  (500–1500 nm) due to the steric hindrance effect. Nanoparticles and nanowire morphologies were also obtained using these ILs. However, the IL 1-n-butyl-2,3-dimethylimidazolium tetrafluoroborate ( $[\text{BDiMIM}][\text{BF}_4]$ ) resulted in only a single morphology (nanoparticles) due to weak hydrogen bonding formed between the imidazolium ring and the oxygen atoms of ZnO. Wang *et al* also used a low-heating solid-state method [110]. They synthesised uniform single-crystal ZnO nanorods in a solid-state  $[\text{C}_4\text{C}_1\text{Im}][\text{BF}_4]$ -sodium hydroxide mixture. The nanorods were characterised

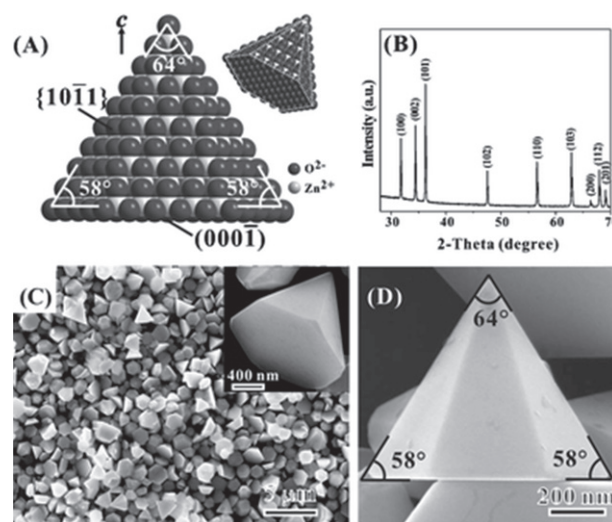


**Figure 10.** (a) Schematic model of a ZnO hexagonal micro-pyramid, (b) x-ray diffraction pattern of ZnO nano/microstructures obtained through IL-assisted thermal decomposition, (c) SEM image of the morphology of ZnO products and an enlarged SEM image (inset), (d) SEM image of an individual ZnO hexagonal micro-pyramid. Reproduced from [111] with permission from the Royal Society of Chemistry.

using a range of experimental techniques including XRD, TEM and XPS. They found that increasing the concentration of sodium hydroxide increased the diameter of the nanorods.

Figure 10 shows ZnO hexagonal micro-pyramids with polar (0001) and  $\{10\bar{1}1\}$  exposed surfaces synthesised using thermal decomposition by Zhou *et al* [111]. They found that strong electrostatic interactions between ILs (consisting of oleic acid and organic amine) and ZnO polar surfaces reduced their surface energy. These would otherwise be energetically unfavourable outer surfaces. The reduced surface energy promotes growth of the crystal along these polar planes, resulting in hexagonal pyramidal structures.

It is common to use zinc acetate as a zinc source for ZnO nanoparticle synthesis [112, 113]. For example, Sabbaghan *et al* used a simple reflux method to synthesise ZnO nanostructures using zinc acetate as a zinc source [97]. They used an imidazolium-based IL-water mixture as a solvent. By controlling the concentration of IL and sodium hydroxide, as well as the cation structure, nanoparticles, nanosheets and nano hollow block morphologies were obtained. They found that increasing the alkyl chain length at position 1 of the imidazolium ring or using a dicationic imidazolium-based IL had the same effect of increasing the width of nanosheets. Using an IL with a smaller alkyl chain led to smaller crystallite sizes. They also found shifts in the optical band gap of the different ZnO morphologies between 2.88–3.16 eV.

A hydrothermal route, using zinc acetate and sodium hydroxide as the reactants, has been used to synthesise rod-like, star-like, and flower-like ZnO nanostructures [114]. The use of a dicationic IL and  $[\text{Zn}(\text{OH})_4]^{2-}$  yielded a 3D flower-like morphology consisting of hexagonal prisms as shown in figure 11. Nanorods grown without ILs showed irregular morphologies, while those grown with ILs were uniform,

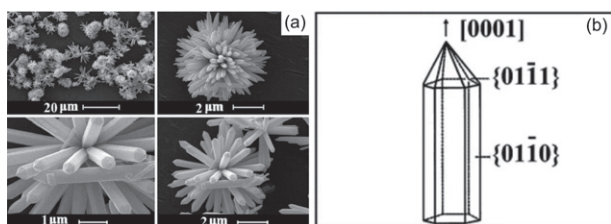


**Figure 11.** (a) SEM images of the flower-like ZnO obtained in the presence of a dicationic IL. (b) The flowers consist of hexagonal prisms that grow along the [0001] direction with a hexagonal pyramid on the tip. Reproduced from [114], with permission from Springer Nature.

revealing the important role of ILs in the fabrication of uniform nanostructures.

### 3.1.2. Interaction of ZnO nanoparticles with ionic liquids.

Surface modification of ZnO nanoparticles with charged IL species can prevent aggregation and formation of nanoparticle clusters. Liu *et al* formed and stabilised ZnO nanocrystals with tunable photoluminescence using an IL with a Zn-based cation [115]. The size, and therefore photoluminescence properties, of the nanocrystals were tuned via changes in the reaction conditions.  $[\text{C}_4\text{C}_1\text{Im}][\text{BF}_4]$ -stabilised ZnO nanocrystals are capable of generating white light through a combination of blue emission from the IL (due to the  $\pi-\pi^*$  transition in the imidazolium-based cation) and yellow emission from defect sites in the ZnO nanocrystals [116].

Sanes *et al* studied the surface interaction between ZnO nanoparticles and  $[\text{C}_6\text{C}_1\text{Im}][\text{PF}_6]$  [117]. Surface modification and reaction of polyhedral nanoparticles with the  $[\text{PF}_6]^-$  anion led to more rounded nanoparticles containing fluorine and phosphorus from the  $[\text{PF}_6]^-$  anion as confirmed by energy-dispersive x-ray spectroscopy. The reaction of ZnO with the  $[\text{PF}_6]^-$  anion also resulted in the formation of nanorods, again, containing fluorine and phosphorus. A third structure came in the form of crystalline needles, mainly consisting of zinc fluoride. These three nanostructures manifested as three distinct peaks in F 1s XPS spectra.

## 3.2. Ionic liquids on ZnO in devices

### 3.2.1. Electric double layer transistors.

It is known that electrolytes, including ILs, can form an electric double layer (EDL) at the surface of semiconductors and charged electrodes. Various models can be used to describe EDL structures such as the Helmholtz, Stern, and Gouy–Chapman models. Usually, IL EDLs consist of alternating layers of cations and anions in what is called a multilayer structure. The IL EDL acts as a nanogap capacitor with very large capacitance [118]. ILs have therefore been used as gate dielectric materials in field-effect transistors (FETs), a configuration called electric double layer transistors (EDLTs). The EDL at the IL/semiconductor interface induces very high charge carrier accumulation, much higher than what is possible in conventional FETs with solid gate dielectrics [118, 119]. Another

benefit is that the IL EDLs form evenly around rough surfaces and nanostructures, producing a uniform gating effect compared to planar gate dielectrics [120].

A range of ILs and semiconducting ZnO nanostructures have been used in EDLTs. For example, Thiemann *et al* demonstrated high electron mobilities in EDLTs using a combination of well-aligned ZnO nanorod thin films and  $[\text{C}_2\text{C}_1\text{Im}][\text{Tf}_2\text{N}]$  [120]. They concluded that electron mobility strongly correlated to the degree of alignment of the nanorods, and less so on their length. The same group also tested the effect of different imidazolium-based ILs as gating electrolytes on the characteristics of EDLTs using spray-deposited polycrystalline ZnO [121]. The capacitance of the IL, as well as size of the anions and cations, was found to influence the electron field-effect mobility. In the same vein, it has been found that decreasing the size of the anion in  $[\text{C}_4\text{C}_1\text{Im}]$ -based ILs ( $[\text{PF}_6]^-$  to  $[\text{BF}_4]^-$ ) results in larger EDL capacitances and faster formation of the EDL due to higher ionic mobility [122]. Meanwhile, the current, threshold voltage and field-effect mobility remain similar.

Yuan *et al* fabricated ZnO EDLTs demonstrating surface polarity recognition, increased accumulated carrier density, and proton memory behaviour by using the protic IL  $[\text{DEME}][\text{Tf}_2\text{N}]$  as a gate dielectric [123]. Under positive gate bias, cations were located at the ZnO anode and anions were located at the Pt cathode, as shown in figure 12. They found that protons and hydroxyls driven to ZnO channel surfaces undergo different absorption mechanisms, showing strong variations in electron transport behaviour. The authors also used the same IL to study electric-field-induced superconductivity in a ZnO EDLT [124]. The  $[\text{DEME}][\text{Tf}_2\text{N}]/\text{ZnO}$  EDLT showed high transconductance and very high carrier densities of  $5.5 \times 10^{14} \text{ cm}^{-2}$  at temperatures as low as 1.8 K.

### 3.2.2. Solar cells.

ILs have also been implemented into ZnO-based solar cells as an electrolyte. Typically in DSSCs, the role of ZnO is to facilitate increased dye absorption, and is usually used in nanoparticulate form. An advantage of using ZnO nanoparticles (compared to  $\text{TiO}_2$  nanoparticles commonly used in DSSCs) is that they require lower annealing temperatures [125]. Other ZnO structures can be used in DSSCs, however, such as porous films. Sheng *et al* used an electro-hydrodynamic technique to fabricate porous ZnO-based DSSCs with an electrolyte mixture composed of  $[\text{C}_3\text{C}_1\text{Im}][\text{I}]$ , iodine, N-methylbenzimidazole and 3-methoxypropionitrile [126]. The use of an IL-based electrolyte led to a high short-circuit current density. Wei *et al* used ZnO nanoparticles for dye molecule anchoring in a flexible IL-based DSSC [125]. The cell consisted of an IL gel electrolyte, organic sensitiser dye, and carbon nanotubes to provide a conductive scaffolding for the growth of ZnO nanoparticles.

Solvent-free DSSCs can be fabricated by using a binary mixture of two ILs, for example,  $[\text{C}_3\text{C}_1\text{Im}][\text{I}]$  and  $[\text{C}_2\text{C}_1\text{Im}][\text{DCA}]$  [85]. In this case, the role of the IL mixture is twofold: (i) the two ILs serve as hole conductors while (ii) one of the ILs also serves as a source of iodide ions (one of the redox couples necessary for dye regeneration).

There are very few computational studies investigating the interfacial interaction between ZnO and ILs for use in solar

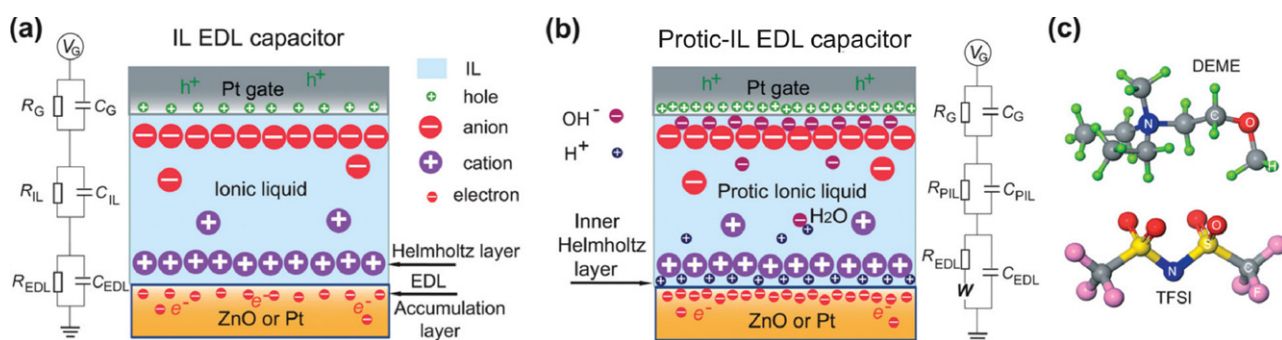


**Figure 12.** Schematic structures of IL and protic ionic liquid (PIL) gated electric double layer (EDL) transistors. (a) Cross section diagram of an IL/solid EDL capacitor and the equivalent circuit. (b) Cross section diagram of a PIL/solid EDL capacitor under a positive gate bias. (c) Molecular structure of the IL [DEME][Tf<sub>2</sub>N]. Reprinted with permission from [123]. Copyright (2010) American Chemical Society.

cells. However, Pandey *et al* recently carried out first-principle DFT calculations of [C<sub>2</sub>C<sub>1</sub>Im][BF<sub>4</sub>] and ZnO nanoclusters as charge-transfer promoters in TiO<sub>2</sub>-based DSSCs [127]. Their computational approach investigated the structural, electronic, and optical properties of [C<sub>2</sub>C<sub>1</sub>Im][BF<sub>4</sub>]/(ZnO)<sub>n</sub> hybrid structures ( $n = 2-12$ ). A decrease in the work function due to [C<sub>2</sub>C<sub>1</sub>Im][BF<sub>4</sub>]/(ZnO)<sub>n</sub> interactions suggests there is charge transfer from ZnO nanoclusters to the IL. The (ZnO)<sub>2</sub> cluster was found to be the most favourable, demonstrating the highest current density, the highest photo-conversion efficiency of 1.96% due to an enhanced electron injection into the TiO<sub>2</sub> layer, improved interfacial contact between the IL and nanocluster, high HOMO energy levels and the most desirable UV-vis characteristics of all clusters tested. [C<sub>2</sub>C<sub>1</sub>Im][BF<sub>4</sub>]/(ZnO)<sub>2</sub> had the highest binding energy between the IL and ZnO nanocluster of all configurations considered, as well as the smallest band gap (3.09 eV).

ILs have also been implemented into other ZnO-based photovoltaic devices. Yu *et al* fabricated inverted polymer solar cells with a very competitive power conversion efficiency of 10.15% [128]. The [C<sub>4</sub>C<sub>1</sub>Im][BF<sub>4</sub>]/ZnO interfacial layer reduced the work function of the cathode and the interfacial energy barrier, thereby increasing the short-circuit current density, fill factor and power conversion efficiency of the solar cell.

A significant challenge to the commercialisation of perovskite solar cells is their long-term instability and degradation in air. This is in part due to surface defects of the perovskite layer and can be combatted by introducing ILs as passivating agents [129]. Alternatively, long-term stability issues can be combatted by improving the quality of the ZnO ETL through surface modification with an IL. Applying [C<sub>4</sub>C<sub>1</sub>Im][BF<sub>4</sub>] between the ZnO ETL and MAPbI<sub>3</sub> perovskite layer was found to increase the power conversion efficiency to 12.1%, compared to 8.59% for unmodified ZnO-based perovskite solar cells [130]. The IL improves surface smoothness of the ZnO layer, leading to increased charge mobility in the ETL, improved charge extraction and reduced photoelectron loss. Zhang *et al* used the passivation effect of [C<sub>2</sub>C<sub>1</sub>Im][PF<sub>6</sub>] on ZnO to improve the long-term stability of a perovskite solar cell in air [131]. The cell (shown schematically in figure 13)

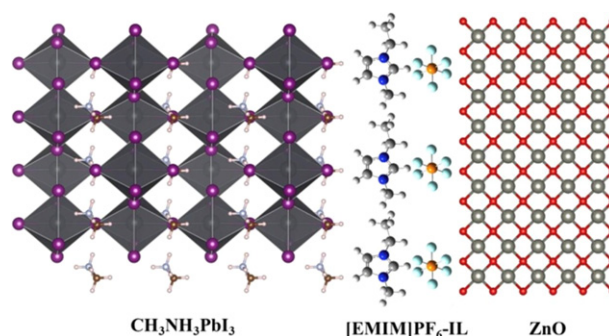


**Figure 13.** Schematic structure of an IL-modified perovskite solar cell where [C<sub>2</sub>C<sub>1</sub>Im][PF<sub>6</sub>] is deposited between a CH<sub>3</sub>NH<sub>3</sub>PbI<sub>3</sub> layer and the ZnO ETL. Reprinted from [131], Copyright (2018), with permission from Elsevier.

retained 88.17% of its initial power conversion efficiency (13.5%) after 90 days of storage in air.

**3.2.3. Other devices and applications.** IL-modified ZnO is desirable for a range of optoelectronic devices thanks to the wide band gap and large exciton binding energy of ZnO (60 meV). Mixing an IL into a ZnO precursor solution can improve the electron injection properties of hybrid organic-inorganic light-emitting diodes [132]. Lee *et al* demonstrated improved performance in hybrid organic-inorganic polymeric LEDs (HyPLEDs) and solar cells (HySCs) via interfacial modification of the ZnO and active polymer layers using the IL 1-benzyl-3-methylimidazolium chloride ([benmim][Cl]) [133]. The device structure is shown in figure 14 [benmim]<sup>+</sup> cations preferentially arranged at the active layer surface while [Cl]<sup>-</sup> anions were located at the ZnO surface. This ionic dipole polarisation within the IL layer reduces the electron injection barrier between the conduction band of ZnO and the LUMO of the active polymer layer. This leads to an enhanced electron injection efficiency in HyPLEDs and a higher open-circuit voltage in HySCs. The electroluminescence efficiency of IL-modified HyPLEDs was found to be 40 times higher than unmodified HyPLEDs.

The photocatalytic properties of ZnO can be investigated and enhanced using ILs. Kowsari and Abdpour used a functional IL precursor to hydrothermally synthesise a

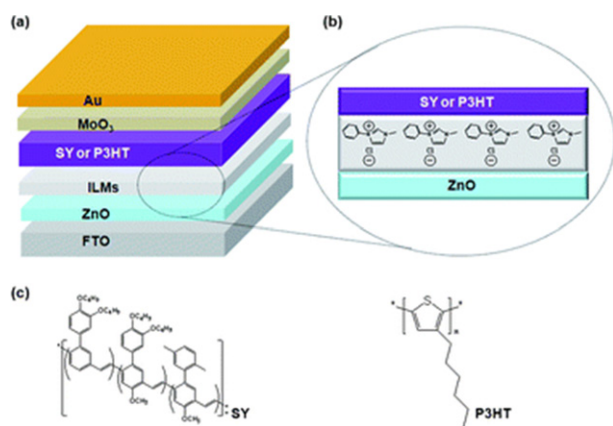


**Figure 14.** (a) Schematic structure of ZnO-based hybrid devices utilising an IL layer. (b) Schematic illustration of [benmim]<sup>+</sup> cations and [Cl]<sup>-</sup> anions between ZnO and the active layer. (c) Chemical structures of super yellow (SY) and poly(3-hexylthiophene) (P3HT). Reproduced from [133] with permission from the Royal Society of Chemistry.

novel hexagonal mesoporous ZnO structure composed of nanoparticles [134]. They studied the photocatalytic degradation of air pollutants and found a maximum of 35%, 56% and 81% removal of CO, NO<sub>x</sub>, and SO<sub>2</sub>, respectively, after 40 min of UV irradiation. Thermal degradation of the IL led to hydroxyl species on the mesoporous ZnO surface. These species have active absorption sites for air pollutants, resulting in improved photocatalytic performance compared to commercial ZnO nanoparticles. Min *et al* fabricated ZnO/graphene heterostructure photocatalysts with visible light response using a [C<sub>4</sub>C<sub>1</sub>Im][PF<sub>6</sub>]-assisting solvothermal method [135]. They obtained a p/n heterojunction interface via the growth of n-type quantum dot sized ZnO nanoparticles on p-type graphene sheets.

ZnO is a biocompatible material that can be used in several biomedical applications, especially in nanoparticulate form. When nanocrystalline ZnO is dispersed in a glycerol/ammonium citrate solution, the nanofluid acts as an effective antibacterial agent against *Escherichia coli* [136]. Thanks to their impressive electrochemical properties, IL-modified ZnO nanoparticles are highly sensitive electrochemical sensors. They are commonly assembled into a nanoparticulate-ZnO/IL/carbon paste electrode configuration (ZnO/IL/CPE) [137]. ZnO/IL/CPEs can be used in voltammetric analysis of anticancer drugs [138]. Pahlavan *et al* synthesised a ZnO/carbon nanotube nanocomposite as a high-sensitivity voltammetric sensor of noradrenaline in pharmaceutical and biological samples using an IL-modified carbon paste electrode [139].

Electrodeposition of metals and semiconductors using ILs is well-established [140] thanks to the wide electrochemical windows and negligible vapour pressures of ILs [141]. Using ILs to electrodeposit metal oxides, however, has been far less explored. Azaceta *et al* used an IL to electrodeposit nanocrystalline ZnO layers [142]. Their approach involved the electrochemical reduction of O<sub>2</sub> in a mixture of zinc bis(trifluoromethanesulfonyl)imide salt and [C<sub>4</sub>C<sub>1</sub>Pyrr][Tf<sub>2</sub>N]

IL. Chemical reaction between Zn<sup>2+</sup> and O<sub>2</sub><sup>-</sup> led to the formation of homogeneous films of ZnO nanocrystals. Addition of the IL was found to affect the crystallite size and the arrangement of primary crystals in nanometre-long agglomerates. Liu *et al* dissolved ZnO in the protic IL 1-methylimidazolium trifluoromethanesulfonate ([C<sub>1</sub>Im][TfO]) at high concentrations (2.5 mol l<sup>-1</sup>) [143]. ZnO/[C<sub>1</sub>Im][TfO] and ZnO/[C<sub>1</sub>Im][TfO]/water solutions were used to electrodeposit highly porous spongy-like zinc structures and compact hexagonal zinc deposits, respectively.

## 4. Ionic liquids on other oxide surfaces

### 4.1. Al<sub>2</sub>O<sub>3</sub> (sapphire) surfaces

Al<sub>2</sub>O<sub>3</sub> (sapphire) surfaces are another popular choice of substrate for the study of ILs. Mezger *et al* studied the structure of three ILs (each containing the [FAP]<sup>-</sup> anion) in contact with a charged Al<sub>2</sub>O<sub>3</sub>(0001) sapphire substrate [144]. Using x-ray reflectivity they found strong interfacial layering, starting with a layer of cations at the negatively charged sapphire surface decaying exponentially into the bulk liquid. The authors suggested that the observed double layer stacking, akin to the charge inversion effect, is expected to be a generic feature of ILs at charged interfaces. However, the ILs which contain a bulky [FAP]<sup>-</sup> anion are rather unusual in structure and size compared to the majority of ILs. Therefore, the same authors investigated two common ILs, [C<sub>4</sub>C<sub>1</sub>Im][PF<sub>6</sub>] and [C<sub>4</sub>C<sub>1</sub>Im][BF<sub>4</sub>], at the charged sapphire interface [145]. They found that [C<sub>4</sub>C<sub>1</sub>Im][PF<sub>6</sub>] shows alternately charged layers of ions decaying exponentially from the surface, in a similar double layer structure as found in their previous study. However, [C<sub>4</sub>C<sub>1</sub>Im][BF<sub>4</sub>], with a smaller anion than [PF<sub>6</sub>], shows a single dense layer at the sapphire interface. They concluded that the interfacial ordering is dependent on IL structure and is dominated by the same electrostatic ion-ion interactions that dominate the bulk correlations.

Akçay *et al* compared the thermal stability limits of bulk ILs to ILs supported on  $\gamma$ -Al<sub>2</sub>O<sub>3</sub> [146]. The nine ILs studied shared a common [C<sub>4</sub>C<sub>1</sub>Im]<sup>+</sup> cation but each had a different anion, such as [Tf<sub>2</sub>N]<sup>-</sup>, [BF<sub>4</sub>]<sup>-</sup> and [TfO]<sup>-</sup>. Thermogravimetric analysis revealed that electronic and structural parameters greatly influence short-term thermal stability limits. They found that increased acidity of the C<sup>2</sup> atom (between the two N atoms in the [C<sub>4</sub>C<sub>1</sub>Im]<sup>+</sup> ring) led to weaker inter-ionic interactions and an increase in thermal stability limits. On the other hand, stronger inter-ionic interactions led to easier thermal decomposition, reducing the thermal stability limits. The authors also found that  $\gamma$ -Al<sub>2</sub>O<sub>3</sub>-supported ILs are thermally stable at significantly lower temperatures compared to bulk ILs. They concluded that interactions between  $\gamma$ -Al<sub>2</sub>O<sub>3</sub> and the IL have a greater impact on thermal stability when cation-anion interactions are weaker.

Lian *et al* used an ionothermal method to synthesise  $\gamma$ -Al<sub>2</sub>O<sub>3</sub> mesoporous nanoflakes using the IL 1-butyl-2,3-dimethylimidazolium chloride, [bdmim][Cl], as a template [147]. The formation mechanism of  $\gamma$ -Al<sub>2</sub>O<sub>3</sub>

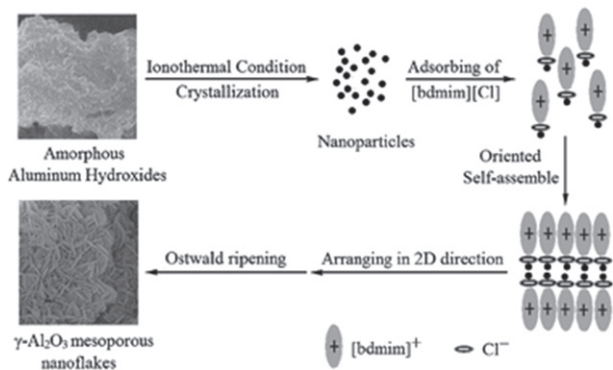


**Figure 15.** Schematic illustration of the formation mechanism of  $\gamma$ - $\text{Al}_2\text{O}_3$  mesoporous nanoflakes using an IL solvent. Reproduced from [147] with permission from the Royal Society of Chemistry.

mesoporous nanoflakes is shown in figure 15 and begins with agglomeration of nanoparticles, which minimises the overall energy of the system. Hydrogen bonding occurs at the interface between  $[\text{Cl}]^-$  anions and  $\text{Al}_2\text{O}_3$   $[\text{bdmim}]^+$  cations also align along the  $\gamma$ - $\text{Al}_2\text{O}_3$  layer due the coulomb coupling force with the anion. Hydrogen bonding and  $\pi$ - $\pi$  interactions between the highly-structured imidazolium rings of  $[\text{bdmim}][\text{Cl}]$  drives the self-assembly of nanoparticles into mesoporous nanoflakes.

#### 4.2. $\text{SnO}_2$ surfaces

Tin oxide ( $\text{SnO}_2$ ) and  $\text{SnO}_2$ /graphene nanocomposites are being considered as alternative anode materials to the commonly used graphite for Li-ion batteries.  $\text{SnO}_2$ /graphene nanocomposites combine the superior theoretical specific capacity of  $\text{SnO}_2$  ( $782 \text{ mAhg}^{-1}$  compared to  $372 \text{ mAhg}^{-1}$  for graphite) with the high electrical conductivity of graphene [148]. Gu *et al* developed an ultrasonic method to embed  $\text{SnO}_2$  nanoparticles on reduced graphene oxide (RGO) using an IL-based solution [149]. The nanocomposite improves device stability during charge–discharge cycles by reducing volume expansion of  $\text{SnO}_2$  nanoparticles and aggregation of  $\text{SnO}_2$  into inactive clusters.

Zhu *et al* used the IL 1-allyl-3-methylimidazolium chloride ( $[\text{Amim}][\text{Cl}]$ ) to synthesise  $\text{SnO}_2$ /graphene nanocomposites using a sol–gel method [150]. They found that the IL interacts with graphene to produce ionic liquid-reduced graphene oxide (IL-RGO) sheets through ‘cation– $\pi$ ’ interactions. The  $[\text{Cl}]^-$  anions of the IL are thought to interact with  $\text{Sn-OH}$  groups through hydrogen bonding while  $[\text{Amim}]^+$  cations interact through  $\pi$ - $\pi$  stacking between imidazolium moieties, as shown in figure 16(b). The IL therefore serves as a ‘glue’ to bind  $\text{SnO}_2$  and graphene sheets into a hybrid structure (denoted  $\text{SnO}_2@$ IL-RGO in figure 16(a)). The self-assembly of  $\text{SnO}_2$  nanoparticles on IL-RGO results in a uniform dispersion, providing more locations for the insertion and extraction of Li ions.

$\text{SnO}_2$ -based Li-ion batteries can be studied *in situ* using high vacuum techniques by exploiting the extremely low vapour pressures of IL electrolytes. Chen *et al* carried out

*in situ* SEM measurements of a  $\text{SnO}_2$  Li-ion battery using the IL  $[\text{C}_4\text{C}_1\text{Pyrr}][\text{Tf}_2\text{N}]$  [151]. They found that the electrochemical behaviour of  $\text{SnO}_2$  is strongly linked to particle size, with larger particles exhibiting surface defects. Similarly, Huang *et al* created a nanoscale battery inside a TEM consisting of a  $\text{SnO}_2$  nanowire anode, a bulk  $\text{LiCoO}_2$  cathode and IL electrolyte [152]. The structural deformation of the single nanowire  $\text{SnO}_2$  anode (fully immersed in an IL-based electrolyte) during lithiation was later studied in detail by the same group [153]. *In situ* TEM images showed that the originally straight nanowire deformed into an amorphous zigzag morphology following initial charging of the battery.

Hollow  $\text{SnO}_2$  structures can be synthesised using ILs and was first achieved by Dong *et al* [154]. They synthesised hollow  $\text{SnO}_2$  nanospheres using  $[\text{C}_4\text{C}_1\text{Im}][\text{BF}_4]$  and a hydrothermal microwave-heating approach. A broader range of  $\text{SnO}_2$  and  $\text{SnO}$  nanostructures have been synthesised since, including nanoparticles [155], microflowers [156], and quantum dots [157].  $\text{SnO}_2$  nanocrystals modified or synthesised by ILs have been studied for other energy storage applications [158], as well as gas sensors [159, 160] and supercapacitors [161].

ILs have been implemented into perovskite solar cells to simultaneously modify the  $\text{SnO}_2$  ETL and passivate the perovskite layer. Huang *et al* modified  $\text{SnO}_2$  nanoparticles using the IL tetramethylammonium hydroxide [162]. The IL enhances the conductivity of the  $\text{SnO}_2$  ETL while also passivating surface and grain boundary defects in the perovskite film. This improves charge transport between perovskite and  $\text{SnO}_2$  layers and enhances electron transport at perovskite grain boundaries.

Chen *et al* used the IL 4-imidazoleacetic acid hydrochloride ( $\text{ImAchCl}$ ) as a multifunctional chemical bridge between a  $\text{SnO}_2$  ETL and perovskite layer [163]. Carboxylic acid groups in  $\text{ImAchCl}$  react with hydroxyl groups on the surface of  $\text{SnO}_2$ , forming ester bonds via esterification. The IL also shifts the conduction and valence bands of  $\text{SnO}_2$  upwards, closer to that of perovskite. Passivation of grain boundary defects in the perovskite film is achieved through electrostatic interactions between the imidazolium cation in  $\text{ImAchCl}$  and iodide anions in perovskite. Interactions with chloride anions were also found to improve the crystallinity of the perovskite film. Their perovskite solar cell modified with  $\text{ImAchCl}$  showed long-term stability and an improved power conversion efficiency of 21% compared to 18% for an unmodified cell.

Recent studies into IL-modified  $\text{SnO}_2$  have extended to flexible perovskite solar cell designs. Liu *et al* fabricated flexible perovskite solar cells with a  $\text{SnO}_2$  ETL and  $[\text{C}_4\text{C}_1\text{Im}][\text{BF}_4]$  interfacial layer [164]. They used DFT calculations to confirm defect passivation in perovskite using  $[\text{C}_4\text{C}_1\text{Im}][\text{BF}_4]$ .

#### 4.3. Other transition and rare-earth metal oxide surfaces

ILs have been used to synthesise a range of transition metal oxide nanoparticles such as iron oxide ( $\text{Fe}_2\text{O}_3$ ) [165–167] and cupric oxide ( $\text{CuO}$ ) [168, 169] using various synthesis methods.

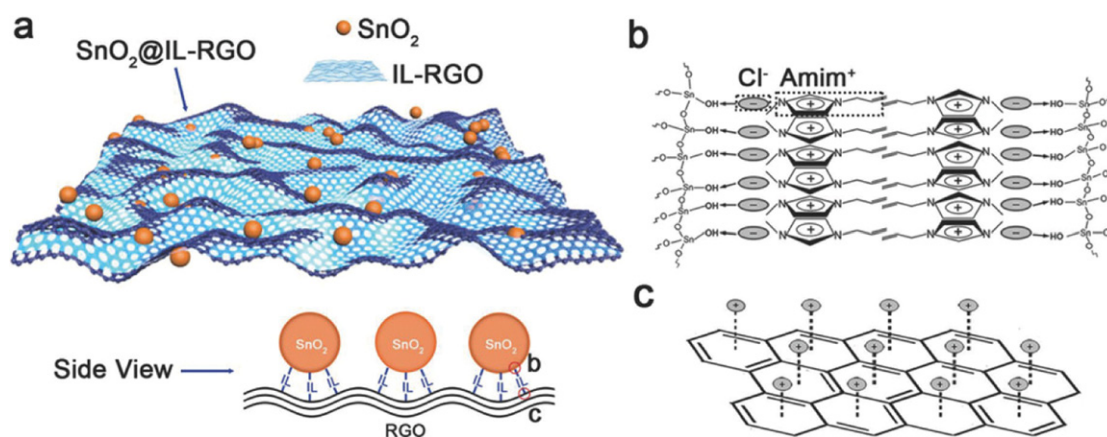


**Figure 16.** (a) Illustration of the SnO<sub>2</sub> and IL-RGO hybrid nanostructure (SnO<sub>2</sub>@IL-RGO). (b) Schematic illustration of the probable hydrogen bond-co- $\pi$ - $\pi$  stack mechanism for the interaction between SnO<sub>2</sub> and IL. (c) Schematic illustration of the probable cation- $\pi$  stack mechanism for the interaction between RGO and IL. [150] John Wiley & Sons. [Copyright © 2018 WILEY-VCH Verlag GmbH & Co. KGaA, Weinheim].

The electrochemical and capacitive properties of a variety of IL-transition metal oxide systems have been evaluated for their use in electrochemical and energy storage devices. An IL-based electrolyte was successfully implemented into a high-voltage MnO<sub>2</sub> asymmetric supercapacitor by Zhang *et al* [170]. The supercapacitor with the highest electrochemical performance used an electrolyte with an equal volume ratio of [C<sub>4</sub>C<sub>1</sub>Im][PF<sub>6</sub>] and N,N-dimethylformamide. Pseudocapacitive behaviour of RuO<sub>2</sub> in a protic IL has been reported by Rochefort and Pont [171]. Cyclic voltammograms revealed distinct redox peaks attributed to Faradaic reactions across the IL-RuO<sub>2</sub> interface, indicative of pseudocapacitance. Double-layer capacitance was observed when the aprotic IL [C<sub>2</sub>C<sub>1</sub>Im][BF<sub>4</sub>] was used instead, yielding a specific capacitance ten times smaller than the electrode in the protic IL.

Zhou and Ramanathan evaluated the electrochemical stability and capacitance of [DEME][Tf<sub>2</sub>N] on VO<sub>2</sub> thin films in an EDLT [172]. The role of an IL electrolyte in a lithium metal battery using V<sub>2</sub>O<sub>5</sub> nanorods, nanowires, and nanoflakes as cathode materials was investigated by Chou *et al* [173]. They found that the IL prevented the dissolution of V<sub>2</sub>O<sub>5</sub> cathode nanomaterials during charging and discharging.

Schernich *et al* studied a thin film of [C<sub>6</sub>C<sub>1</sub>Im][Tf<sub>2</sub>N] on ordered stoichiometric CeO<sub>2</sub>(111) and partially reduced CeO<sub>2-x</sub> using photoelectron spectroscopy [174]. On CeO<sub>2-x</sub> they observed decomposition of the anion. On the CeO<sub>2</sub>(111) surface they found that a layer of organic products with high thermal stability was formed upon reaction of the cation. The same group then studied the effect of oxo-functionalisation of the IL on its interaction with these surfaces [175]. They found that the oxo-functionalised [5-oxo-C<sub>6</sub>C<sub>1</sub>Im][Tf<sub>2</sub>N] adsorbs molecularly onto both oxides at low temperature. With the non-functionalised IL they found the alkyl chain oriented towards the vacuum but with the oxo-functionalised IL the alkyl chain orientated parallel to the surface, due to the interaction of the carbonyl group with the surfaces. Upon heating the IL decomposes on both surfaces and the authors provide a reaction and decomposition scheme as shown in figure 17. Their work shows that by adding functional groups to the IL

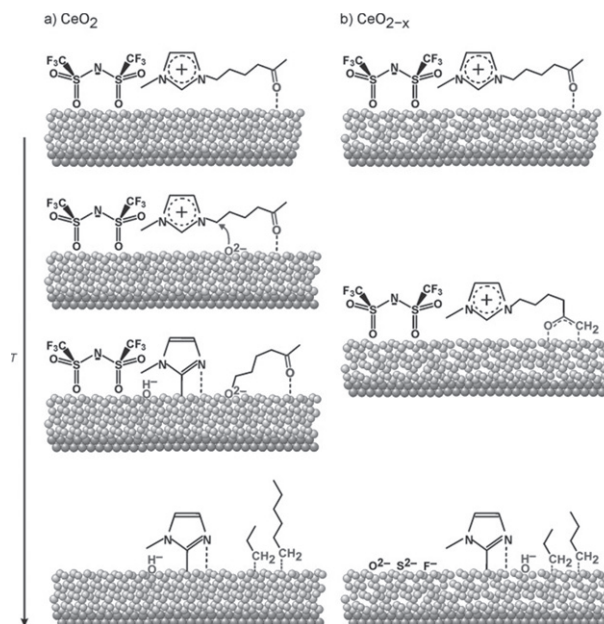


**Figure 17.** Schematic summary of the main steps identified upon reaction and decomposition of [5-oxo-C<sub>6</sub>C<sub>1</sub>Im][Tf<sub>2</sub>N] on (a) a stoichiometric CeO<sub>2</sub> surface and (b) a partially reduced CeO<sub>2-x</sub> surface. [175] John Wiley & Sons. [Copyright © 2013 WILEY-VCH Verlag GmbH & Co. KGaA, Weinheim].

it is possible to tune its interaction and molecular ordering on the oxide surface.

Cremer *et al* studied ultrathin films of [C<sub>1</sub>C<sub>1</sub>Im][Tf<sub>2</sub>N] on clean, oxygen precovered and oxidised Ni(111) single crystal surfaces using angle-resolved XPS [18]. Their results indicate that on clean Ni(111) at submonolayer coverages, a sandwich structure is formed, with the cation in contact with the surface and the anion on top. This transitions to a checkerboard-type structure at higher coverages, with the anions and cations next to each other. On the oxygen precovered O ( $\sqrt{3} \times \sqrt{3}$ ) R30° Ni(111) surface the checkerboard arrangement is preferred. In thermal stability studies they found that on the clean Ni(111) surface the IL adsorption was reversible upon heating. For

the oxidised NiO surface, irreversible decomposition of the IL occurs upon heating. They found that cation-related moieties can desorb from the surface but anion-related moieties remain on the surface to much higher temperatures. This study demonstrates how the properties of the oxide substrate can strongly influence the adsorption, orientation and chemical reactivity of the IL.

Migowski *et al* used a number of imidazolium-based ILs to prepare nanoparticles with a Ni core and a NiO outer shell [176]. The diameter and size-distribution of the Ni nanoparticles were reduced by increasing the length of the alkyl side-chain ( $n = 4, 8, 10, 14$ ) of the imidazolium ring in  $[C_nC_1Im][Tf_2N]$ , before increasing again for  $n = 16$ . The NiO:Ni ratio was found to increase from  $n = 4$  to 8, before decreasing when the number of carbon atoms in the alkyl chain increased further.

#### 4.4. Comparative studies across oxide surfaces

Babucci *et al* investigated the thermal stability limits of 33 imidazolium ILs immobilised on high surface area metal oxides  $SiO_2$ ,  $\gamma-Al_2O_3$ , MgO [177]. They found that systematic changes such as the size of the cation/anion, methylation on the carbon at position 2 of the imidazolium ring, and substitution of alkyl groups on the imidazolium ring with functional groups have significant effects on thermal stability limits. Supported ILs typically have a lower thermal stability than the bulk IL. Generally, they found that as the point of zero charge (PZC) of the metal oxide increases from  $SiO_2$  to MgO, the interactions between the IL and metal oxide surface dominate over interionic interactions, and the surface becomes the significant factor in controlling the stability limits. The same group studied interactions between  $[C_4C_1Im][BF_4]$  with a wider range of high-surface-area metal oxides,  $SiO_2$ ,  $TiO_2$ ,  $Fe_2O_3$ , ZnO,  $\gamma-Al_2O_3$ ,  $CeO_2$ , MgO, and  $La_2O_3$  using infrared spectroscopy and DFT calculations [178]. These metal oxide surfaces covered a wide range of PZCs from pH = 2 to 11. Their results show that the surface acidity strongly controls the IL/surface interactions and that thermal stability limits significantly decrease with increasing PZC of the metal oxide surface. Their results are useful in choosing suitable ILs and surfaces to withstand the operating conditions in applications such as SCILL or SILP catalysis.

## 5. Conclusion and outlook

In this review, the interfacial behaviour and interactions of ILs at single crystal and nanoparticulate oxide surfaces have been explored, with a view towards potential applications and devices. IL adsorbates on oxide surfaces exhibit interesting electrochemical, optical, and capacitive behaviour, and their ions often demonstrate self-assembly and ordering at the surface. Most of these properties are highly controllable by choice of the cation/anion pair and length of alkyl side chains in imidazolium-based ILs. Key characteristics of IL/oxide systems have been discussed and are found to be underpinned

by a rich and complex interplay of intermolecular, electrostatic, physical, and chemical interactions occurring at the interface.

We have explored  $TiO_2$  and ZnO in particular detail due to their use alongside ILs across an expansive range of potential applications and devices. These include, but are not limited to, solar cells, catalysts, batteries, supercapacitors, transistors, gas capture and storage, lubrication, and nanoparticle synthesis. There is a wealth of research and evidence indicating that ILs have a promising future for commercial and industrial use. There are, however, still a number of challenges that hinder the commercialisation of IL-based technologies.

A major limitation for DSSC commercialisation is the compromise between efficiency and long-term stability. The use of IL electrolytes has been found to improve the longevity and thermal stability of DSSCs, but this usually comes at the cost of lower power conversion efficiencies (<10%) compared to electrolytes containing organic solvents [9, 179]. In perovskite solar cells, ILs have been used as additives to perovskite precursors in order to enhance the crystallinity of the perovskite layer. However, there are still very few studies investigating the interaction between the IL and perovskite precursors (such as IL anions and  $PbI_2$ ) [180, 181].

ILs have been shown to significantly reduce the energy consumption of carbon capture technologies compared to conventional amine-based solvents [182]. However, they still face some economic challenges such as high synthesis costs [183]. It is therefore necessary to design low-cost but high-performance ILs if they are to see use in a widescale industrial capacity. There are also very few fundamental studies probing the influence of gases on the behaviour of ILs at oxide surfaces which could consequently affect their performance in many of the applications described [38].

It is clear that improving our understanding of the fundamental interactions between ILs and oxide surfaces is crucial for designing and commercialising efficient, eco-friendly, high-performance, and stable devices.

## Acknowledgments

The authors acknowledge the Jeremiah Horrocks Institute for the PhD studentship for Jordan Cole.

## Data availability statement

No new data were created or analysed in this study.

## ORCID iDs

Jordan Cole  <https://orcid.org/0000-0002-0325-2049>

Karen L Syres  <https://orcid.org/0000-0001-7439-475X>

## References

- [1] Huang J and R  ther T 2009 *Aust. J. Chem.* **62** 298–308
- [2] Giernoth R 2010 *Angew. Chem., Int. Ed.* **49** 2834–9
- [3] Welton T 2004 *Coord. Chem. Rev.* **248** 2459–77

- [4] Steinrück H P and Wasserscheid P 2015 *Catal. Lett.* **145** 380–97
- [5] Lewandowski A and Świdarska-Mocek A 2009 *J. Power Sources* **194** 601–9
- [6] Eftekhari A, Liu Y and Chen P 2016 *J. Power Sources* **334** 221–39
- [7] Somers A, Howlett P, MacFarlane D and Forsyth M 2013 *Lubricants* **1** 3–21
- [8] Zhou F, Liang Y and Liu W 2009 *Chem. Soc. Rev.* **38** 2590–9
- [9] Abu Talip R A, Yahya W Z N and Bustam M A 2020 *Sustainability* **12** 7598
- [10] Zhao Y and Bostrom T 2015 *Curr. Org. Chem.* **19** 556–66
- [11] Lockett V, Sedev R, Bassell C and Ralston J 2008 *Phys. Chem. Chem. Phys.* **10** 1330–5
- [12] Iwahashi T, Nishi T, Yamane H, Miyamae T, Kanai K, Seki K, Kim D and Ouchi Y 2009 *J. Phys. Chem. C* **113** 19237–43
- [13] Carstens T, Hayes R, Abedin S Z E, Corr B, Webber G B, Borisenko N, Atkin R and Endres F 2012 *Electrochim. Acta* **82** 48–59
- [14] Cremer T, Stark M, Deyko A, Steinrück H-P and Maier F 2011 *Langmuir* **27** 3662–71
- [15] Syres K L and Jones R G 2015 *Langmuir* **31** 9799–808
- [16] Foulston R, Gangopadhyay S, Chiutu C, Moriarty P and Jones R G 2012 *Phys. Chem. Chem. Phys.* **14** 6054–66
- [17] McIntosh E M, Ellis J, Jardine A P, Licence P, Jones R G and Allison W 2014 *Chem. Sci.* **5** 667–76
- [18] Cremer T, Wibmer L, Calderón S K, Deyko A, Maier F and Steinrück H-P 2012 *Phys. Chem. Chem. Phys.* **14** 5153–63
- [19] Uhl B, Buchner F, Gabler S, Bozorgchenani M and Jürgen Behm R 2014 *Chem. Commun.* **50** 8601–4
- [20] Klaver T P C, Luppi M, Sluiter M H F, Kroon M C and Thijssse B J 2011 *J. Phys. Chem. C* **115** 14718–30
- [21] Freund H-J, Kuhlbeck H and Staemmler V 1996 *Rep. Prog. Phys.* **59** 283–347
- [22] O'Regan B and Grätzel M 1991 *Nature* **353** 737–40
- [23] Calisir M D, Stojanovska E and Kilic A 2018 13 - Polymer nanocomposites for dye-sensitized solar cells *Polymer-based Nanocomposites for Energy and Environmental Applications* (Amsterdam: Elsevier) <https://doi.org/10.1016/B978-0-08-102262-7.00013-1>
- [24] Sahli F *et al* 2018 *Nat. Mater.* **17** 820–6
- [25] Yoo J J *et al* 2021 *Nature* **590** 587–93
- [26] Steinrück H P *et al* 2011 *Adv. Mater.* **23** 2571–87
- [27] Minami I 2009 *Molecules* **14** 2286–305
- [28] Liu X, Ma J and Zheng W 2011 *Rev. Adv. Mater. Sci.* **27** 43]–51
- [29] Lazzeri M, Vittadini A and Selloni A 2001 *Phys. Rev. B* **63** 155409
- [30] Zhang J, Zhou P, Liu J and Yu J 2014 *Phys. Chem. Chem. Phys.* **16** 20382–6
- [31] Weber H, Salanne M and Kirchner B 2015 *J. Phys. Chem. C* **119** 25260–7
- [32] Weber H, Bredow T and Kirchner B 2015 *J. Phys. Chem. C* **119** 15137–49
- [33] Weber H and Kirchner B 2016 *ChemSusChem* **9** 2505–14
- [34] Wagstaffe M, Jackman M J, Syres K L, Generalov A and Thomas A G 2016 *ChemPhysChem* **17** 3430–4
- [35] Liu L, Li S, Cao Z, Peng Y, Li G, Yan T and Gao X-P 2007 *J. Phys. Chem. C* **111** 12161–4
- [36] Malali S and Foroutan M 2017 *J. Phys. Chem. C* **121** 11226–33
- [37] Henderson Z, Walton A S, Thomas A G and Syres K L 2018 *J. Phys.: Condens. Matter* **30** 334003
- [38] Cole J *et al* 2021 *J. Phys. Chem. C* **125** 22778–85
- [39] Uhl B, Hekmatfar M, Buchner F and Behm R J 2016 *Phys. Chem. Chem. Phys.* **18** 6618–36
- [40] Kroon M C, Buijs W, Peters C J and Witkamp G-J 2006 *Green Chem.* **8** 241–5
- [41] Howlett P C, Izgorodina E I, Forsyth M and MacFarlane D R 2006 *Z. Phys. Chem.* **220** 1483–98
- [42] Kroon M C, Buijs W, Peters C J and Witkamp G-J 2007 *Thermochim. Acta* **465** 40–7
- [43] Suzuki S, Ohta Y, Kurimoto T, Kuwabata S and Torimoto T 2011 *Phys. Chem. Chem. Phys.* **13** 13585–93
- [44] Nakashima T and Kimizuka N 2003 *J. Am. Chem. Soc.* **125** 6386–7
- [45] Ding K, Miao Z, Liu Z, Zhang Z, Han B, An G, Miao S and Xie Y 2007 *J. Am. Chem. Soc.* **129** 6362–3
- [46] Feng X-t and Liu C-y 2010 *J. Am. Ceram. Soc.* **93** 1845–7
- [47] Li H, Qu J, Cui Q, Xu H, Luo H, Chi M, Meisner R A, Wang W and Dai S 2011 *J. Mater. Chem.* **21** 9487–90
- [48] Paramasivam I, Macak J M, Selvam T and Schmuki P 2008 *Electrochim. Acta* **54** 643–8
- [49] Mali S S, Betty C A, Bhosale P N, Devan R S, Ma Y-R, Kolekar S S and Patil P S 2012 *CrystEngComm* **14** 1920
- [50] Shahi S K, Kaur N and Singh V 2016 *Appl. Surf. Sci.* **360** 953–60
- [51] Chang H-C, Hung T-C, Chang S-C, Jiang J-C and Lin S H 2011 *J. Phys. Chem. C* **115** 11962–7
- [52] Gindri I M, Frizzo C P, Bender C R, Tier A Z, Martins M A P, Villetti M A, MacHado G, Rodriguez L C and Rodrigues D C 2014 *ACS Appl. Mater. Interfaces* **6** 11536–43
- [53] Aliaga C and Baldelli S 2008 *J. Phys. Chem. C* **112** 3064–72
- [54] An R, Zhu Y, Wu N, Xie W, Lu J, Feng X and Lu X 2013 *ACS Appl. Mater. Interfaces* **5** 2692–8
- [55] Puxty G, Rowland R and Attalla M 2010 *Chem. Eng. Sci.* **65** 915–22
- [56] Fabregat-Santiago F, Randriamahazaka H, Zaban A, Garcia-Cañadas J, Garcia-Belmonte G and Bisquert J 2006 *Phys. Chem. Chem. Phys.* **8** 1827–33
- [57] Binetti E, Panniello A, Tommasi R, Agostiano A, Fantini S, Curri M L and Striccoli M 2013 *J. Phys. Chem. C* **117** 12923–9
- [58] Zhang S, Zhang J, Zhang Y and Deng Y 2017 *Chem. Rev.* **117** 6755–833
- [59] Perkin S 2012 *Phys. Chem. Chem. Phys.* **14** 5052–62
- [60] Ueno K, Kasuya M, Watanabe M, Mizukami M and Kurihara K 2010 *Phys. Chem. Chem. Phys.* **12** 4066–71
- [61] Lian S, Song C, Liu Q, Duan E, Ren H and Kitamura Y 2021 *J. Environ. Sci.* **99** 281–95
- [62] Coasne B, Viau L and Vioux A 2011 *J. Phys. Chem. Lett.* **2** 1150–4
- [63] Verma Y L, Singh M P and Singh R K 2012 *Mater. Lett.* **86** 73–6
- [64] Singh R, Rajput N N, He X, Monk J and Hung F R 2013 *Phys. Chem. Chem. Phys.* **15** 16090–103
- [65] Rajput N N, Monk J, Singh R and Hung F R 2012 *J. Phys. Chem. C* **116** 5169–81
- [66] Shen Y, He X and Hung F R 2015 *J. Phys. Chem. C* **119** 24489–500
- [67] Papageorgiou N, Athanassov Y, Armand M, Bonhôte P, Pettersson H, Azam A and Grätzel M 1996 *J. Electrochem. Soc.* **143** 3099–108
- [68] Kuang D, Wang P, Ito S, Zakeeruddin S M and Grätzel M 2006 *J. Am. Chem. Soc.* **128** 7732–3
- [69] Kuang D, Klein C, Zhang Z, Ito S, Moser J-E, Zakeeruddin S M and Grätzel M 2007 *Small* **3** 2094–102
- [70] Gao F *et al* 2008 *J. Am. Chem. Soc.* **130** 10720–8
- [71] Zhang C, Huang Y, Huo Z, Chen S and Dai S 2009 *J. Phys. Chem. C* **113** 21779–83
- [72] Singh P K, Kim K-W, Park N-G and Rhee H-W 2008 *Synth. Met.* **158** 590–3
- [73] Wang P, Zakeeruddin S M, Exnar I and Grätzel M 2002 *Chem. Commun.* **24** 2972–3
- [74] Hashmi S G, Ozkan M, Halme J, Misic K D, Zakeeruddin S M, Paltakari J, Grätzel M and Lund P D 2015 *Nano Energy* **17** 206–15
- [75] Murai S, Mikoshiba S, Sumino H, Kato T and Hayase S 2003 *Chem. Commun.* **3** 1534–5

- [76] Kubo W, Kitamura T, Hanabusa K, Wada Y and Yanagida S 2002 *Chem. Commun.* **4** 374–5
- [77] Wang P, Zakeeruddin S M, Comte P, Exnar I and Grätzel M 2003 *J. Am. Chem. Soc.* **125** 1166–7
- [78] Yamanaka N, Kawano R, Kubo W, Masaki N, Kitamura T, Wada Y, Watanabe M and Yanagida S 2007 *J. Phys. Chem. B* **111** 4763–9
- [79] Bai Y, Zhang J, Wang Y, Zhang M and Wang P 2011 *Langmuir* **27** 4749–55
- [80] Zhang M, Zhang J, Bai Y, Wang Y, Su M and Wang P 2011 *Phys. Chem. Chem. Phys.* **13** 3788–94
- [81] Yang D, Zhou X, Yang R, Yang Z, Yu W, Wang X, Li C, Liu S and Chang R P H 2016 *Energy Environ. Sci.* **9** 3071–8
- [82] Seo J-Y *et al* 2016 *Adv. Energy Mater.* **6** 1600767
- [83] Shahiduzzaman M *et al* 2017 *Org. Electron.* **48** 147–53
- [84] Bai S *et al* 2019 *Nature* **571** 245–50
- [85] Guillén E, Fernández-Lorenzo C, Alcántara R, Martín-Calleja J and Anta J A 2009 *Sol. Energy Mater. Sol. Cells* **93** 1846–52
- [86] Mane R S, Lee W J, Pathan H M and Han S-H 2005 *J. Phys. Chem. B* **109** 24254–9
- [87] Özgür Ü, Alivov Y I, Liu C, Teke A, Reshchikov M A, , Doğan S, Avrutin V, Cho S-J and Morkoç H 2005 *J. Appl. Phys.* **98** 041301
- [88] Hernández S, Hidalgo D, Sacco A, Chiodoni A, Lamberti A, Cauda V, Tresso E and Saracco G 2015 *Phys. Chem. Chem. Phys.* **17** 7775–86
- [89] Lin C-Y, Lai Y-H, Chen H-W, Chen J-G, Kung C-W, Vittal R and Ho K-C 2011 *Energy Environ. Sci.* **4** 3448–855
- [90] Ko S H, Lee D, Kang H W, Nam K H, Yeo J Y, Hong S J, Grigoropoulos C P and Sung H J 2011 *Nano Lett.* **11** 666–71
- [91] Georgekutty R, Seery M K and Pillai S C 2008 *J. Phys. Chem. C* **112** 13563–70
- [92] Chen X, Wu Z, Liu D and Gao Z 2017 *Nanoscale Res. Lett.* **12** 4–13
- [93] Kim K-S, Demberelnyamba D and Lee H 2004 *Langmuir* **20** 556–60
- [94] Movlaroooy T 2018 *Mater. Res. Express* **5** 035032
- [95] Ahmed T and Edvinsson T 2020 *J. Phys. Chem. C* **124** 6395–404
- [96] Wang N, Yang Y and Yang G 2011 *Nanoscale Res. Lett.* **6** 2–7
- [97] Sabbaghan M, Shahvelayati A S and Bashtani S E 2012 *Solid State Sci.* **14** 1191–5
- [98] Wang L, Chang L, Zhao B, Yuan Z, Shao G and Zheng W 2008 *Inorg. Chem.* **47** 1443–52
- [99] Sabbaghan M, Beheshtian J and Mirsaedi S A M 2014 *Ceram. Int.* **40** 7769–74
- [100] Wang L, Xu S-Z, Li H-J, Chang L-X, Zhi-Su , Zeng M-H, Wang L-N and Huang Y-N 2011 *J. Solid State Chem.* **184** 720–4
- [101] Rabieh S, Bagheri M, Heydari M and Badiei E 2014 *Mater. Sci. Semicond. Process.* **26** 244–50
- [102] Li Z, Jia Z, Luan Y and Mu T 2008 *Curr. Opin. Solid State Mater. Sci.* **12** 1–8
- [103] Wang W-W and Zhu Y-J 2004 *Inorg. Chem. Commun.* **7** 1003–5
- [104] Wang J, Cao J, Fang B, Lu P, Deng S and Wang H 2005 *Mater. Lett.* **59** 1405–8
- [105] Xu H, Zeiger B W and Suslick K S 2013 *Chem. Soc. Rev.* **42** 2555–67
- [106] Goharshadi E K, Ding Y, Jorabchi M N and Nancarrow P 2009 *Ultrason. Sonochem.* **16** 120–3
- [107] Morris R E 2009 *Chem. Commun.* **21** 2990–8
- [108] Zhu H, Huang J-F, Pan Z and Dai S 2006 *Chem. Mater.* **18** 4473–7
- [109] Zhang J, Wang J, Zhou S, Duan K, Feng B, Weng J, Tang H and Wu P 2010 *J. Mater. Chem.* **20** 9798–804
- [110] Wang L, Zhao B, Chang L and Zheng W 2007 *Sci. China B* **50** 224–9
- [111] Zhou X, Xie Z-X, Jiang Z-Y, Kuang Q, Zhang S-H, Xu T, Huang R-B and Zheng L-S 2005 *Chem. Commun.* **2005** 5572–4
- [112] Luo B, Rossini J E and Gladfelter W L 2009 *Langmuir* **25** 13133–41
- [113] Li Z, Geßner A, Richters J-P, Kalden J, Voss T, Kübel C and Taubert A 2008 *Adv. Mater.* **20** 1279–85
- [114] Yavari I, Mahjoub A R, Kowsari E and Movahedi M 2009 *J. Nanoparticle Res.* **11** 861–8
- [115] Liu D-P, Li G-D, Su Y and Chen J-S 2006 *Angew. Chem., Int. Ed.* **45** 7370–3
- [116] Kar A, Kundu S and Patra A 2012 *RSC Adv.* **2** 4879–85
- [117] Sanes J, Carrión F-J and Bermúdez M-D 2009 *Appl. Surf. Sci.* **255** 4859–62
- [118] Yuan H, Shimotani H, Ye J, Yoon S, Aliah H, Tsukazaki A, Kawasaki M and Iwasa Y 2010 *J. Am. Chem. Soc.* **132** 18402–7
- [119] Fujimoto T and Awaga K 2013 *Phys. Chem. Chem. Phys.* **15** 8983–9006
- [120] Thiemann S, Gruber M, Lokteva I, Hirschmann J, Halik M and Zausseil J 2013 *ACS Appl. Mater. Interfaces* **5** 1656–62
- [121] Thiemann S, Sachnov S, Porscha S, Wasserscheid P and Zausseil J 2012 *J. Phys. Chem. C* **116** 13536–44
- [122] Singh M, Manoli K, Tiwari A, Ligonzo T, Di Franco C, , Cioffi N, Palazzo G, Scamarcio G and Torsi L 2017 *J. Mater. Chem. C* **5** 3509–18
- [123] Yuan H, Shimotani H, Tsukazaki A, Ohtomo A, Kawasaki M and Iwasa Y 2010 *J. Am. Chem. Soc.* **132** 6672–8
- [124] Yuan H, Shimotani H, Tsukazaki A, Ohtomo A, Kawasaki M and Iwasa Y 2009 *Adv. Funct. Mater.* **19** 1046–53
- [125] Wei D, Unalan H E, Han D, Zhang Q, Niu L, Amaratunga G and Ryhanen T 2008 *Nanotechnology* **19** 424006
- [126] Sheng X, Zhao Y, Zhai J, Jiang L and Zhu D 2007 *Appl. Phys. A* **87** 715–9
- [127] Pandey D K, Kagdada H L, Materny A and Singh D K 2021 *J. Mol. Liq.* **322** 114538
- [128] Yu W, Huang L, Yang D, Fu P, Zhou L, Zhang J and Li C 2015 *J. Mater. Chem. A* **3** 10660–5
- [129] Zhu X *et al* 2021 *Angew. Chem., Int. Ed.* **60** 4238–44
- [130] Chu W, Yang J, Jiang Q, Li X and Xin J 2018 *Appl. Surf. Sci.* **440** 1116–22
- [131] Zhang W, Ren Z, Guo Y, He X and Li X 2018 *Electrochim. Acta* **268** 539–45
- [132] Brine H, Sánchez-Royo J F and Bolink H J 2013 *Org. Electron.* **14** 164–8
- [133] Lee B R, Choi H, Sunpark J, Lee H J, Kim S O, Kim J Y and Song M H 2011 *J. Mater. Chem.* **21** 2051–3
- [134] Kowsari E and Abdpour S 2017 *J. Solid State Chem.* **256** 141–50
- [135] Min Y, Zhang K, Chen L, Chen Y and Zhang Y 2012 *Diam. Relat. Mater.* **26** 32–8
- [136] Jalal R, Goharshadi E K, Abareshi M, Moosavi M, Yousefi A and Nancarrow P 2010 *Mater. Chem. Phys.* **121** 198–201
- [137] Karimi-Maleh H, Rostami S, Gupta V K and Fouladgar M 2015 *J. Mol. Liq.* **201** 102–7
- [138] Alavi-Tabari S A R, Khalilzadeh M A and Karimi-Maleh H 2018 *J. Electroanal. Chem.* **811** 84–8
- [139] Pahlavan A, Gupta V K, Sanati A L, Karimi F, Yoosefian M and Ghadami M 2014 *Electrochim. Acta* **123** 456–62
- [140] Endres F 2002 *ChemPhysChem* **3** 144–54
- [141] Armand M, Endres F, MacFarlane D R, Ohno H and Scrosati B 2009 *Nat. Mater.* **8** 621–9
- [142] Azaceta E, Tena-Zaera R, Marcilla R, Fantini S, , Echeberria J, Pomposo J A, Grande H and Mecerreyes D 2009 *Electrochem. Commun.* **11** 2184–6

- [143] Liu Z, El Abedin S Z and Endres F 2015 *Electrochem. Commun.* **58** 46–50
- [144] Mezger M *et al* 2008 *Science* **322** 424–8
- [145] Mezger M *et al* 2009 *J. Chem. Phys.* **131** 094701
- [146] Akçay A, Balci V and Uzun A 2014 *Thermochim. Acta* **589** 131–6
- [147] Lian J, Ma J, Duan X, Kim T, Li H and Zheng W 2010 *Chem. Commun.* **46** 2650–2
- [148] Lian P, Zhu X, Liang S, Li Z, Yang W and Wang H 2011 *Electrochimica Acta* **56** 4532–9
- [149] Gu C, Zhang H, Wang X and Tu J 2013 *Mater. Res. Bull.* **48** 4112–7
- [150] Zhu S, Dong X, Gao S, Jin X, Huang H and Qi M 2018 *Adv. Mater. Interfaces* **5** 1701685
- [151] Chen D, Indris S, Schulz M, Gamer B and Mönig R 2011 *J. Power Sources* **196** 6382–7
- [152] Huang J Y *et al* 2010 *Science* **330** 1515–20
- [153] Wang C-M *et al* 2011 *Nano Lett.* **11** 1874–80
- [154] Dong W-S, Li M-Y, Liu C, Lin F and Liu Z 2008 *J. Colloid Interface Sci.* **319** 115–22
- [155] Taghvaei V, Habibi-Yangjeh A and Behboudnia M 2009 *Powder Technol.* **195** 63–7
- [156] Qin B, Zhang H, Diemant T, Geiger D, Raccichini R, Behm R J, Kaiser U, Varzi A and Passerini S 2017 *ACS Appl. Mater. Interfaces* **9** 26797–804
- [157] Xiao L, Shen H, von Hagen R, Pan J, Belkoura L and Mathur S 2010 *Chem. Commun.* **46** 6509
- [158] Dutta B, Deb D and Bhattacharya S 2018 *Int. J. Hydrog. Energy* **43** 4081–9
- [159] Li R, Du J, Luan Y, Zou H, Zhuang G and Li Z 2012 *CrytEngComm* **14** 3404
- [160] Li L-L, Zhang W-M, Yuan Q, Li Z-X, Fang C-J, Sun L-D, Wan L-J and Yan C-H 2008 *Cryst. Growth Des.* **8** 4165–72
- [161] Nguyen V H and Shim J-J 2015 *Synth. Met.* **207** 110–5
- [162] Huang C *et al* 2018 *J. Mater. Chem. A* **6** 22086–95
- [163] Chen J, Zhao X, Kim S G and Park N G 2019 *Adv. Mater.* **31** 1902902
- [164] Liu D, Zheng H, Ahmed Y, Zheng C, Wang Y, Chen H, Chen L and Li S 2022 *J. Power Sources* **519** 230814
- [165] Lian J, Duan X, Ma J, Peng P, Kim T and Zheng W 2009 *ACS Nano* **3** 3749–61
- [166] Wang Y and Yang H 2009 *Chem. Eng. J.* **147** 71–8
- [167] Lee C-M, Jeong H-J, Lim S T, Sohn M-H and Kim D W 2010 *ACS Appl. Mater. Interfaces* **2** 756–9
- [168] Xu X, Zhang M, Feng J and Zhang M 2008 *Mater. Lett.* **62** 2787–90
- [169] Zhang M, Xu X and Zhang M 2008 *Mater. Lett.* **62** 385–8
- [170] Zhang X, Zhao D, Zhao Y, Tang P, Shen Y, Xu C, Li H and Xiao Y 2013 *J. Mater. Chem. A* **1** 3706–12
- [171] Rochefort D and Pont A-L 2006 *Electrochem. Commun.* **8** 1539–43
- [172] Zhou Y and Ramanathan S 2012 *J. Appl. Phys.* **111** 084508
- [173] Chou S-L, Wang J-Z, Sun J-Z, Wexler D, Forsyth M, Liu H-K, MacFarlane D R and Dou S-X 2008 *Chem. Mater.* **20** 7044–51
- [174] Schernich S *et al* 2013 *J. Phys. Chem. Lett.* **4** 30–5
- [175] Schernich S *et al* 2013 *ChemPhysChem* **14** 3673–7
- [176] Migowski P, Machado G, Teixeira S R, Alves M C M, Morais J, Traverse A and Dupont J 2007 *Phys. Chem. Chem. Phys.* **9** 4814–21
- [177] Babucci M, Akçay A, Balci V and Uzun A 2015 *Langmuir* **31** 9163–76
- [178] Babucci M, Balci V, Akçay A and Uzun A 2016 *J. Phys. Chem. C* **120** 20089–102
- [179] Wang P *et al* 2018 *Joule* **2** 2145–53
- [180] Wang J, Ye X, Wang Y, Wang Z, Wong W and Li C 2019 *Electrochim. Acta* **303** 133–9
- [181] Zhang Y, Fei Z, Gao P, Lee Y, Tirani F F, Scopelliti R, Feng Y, Dyson P J and Nazeeruddin M K 2017 *Adv. Mater.* **29** 1702157
- [182] Liu X, Huang Y, Zhao Y, Gani R, Zhang X and Zhang S 2016 *Ind. Eng. Chem. Res.* **55** 5931–44
- [183] Aghaie M, Rezaei N and Zendeheboudi S 2018 *Renew. Sustain. Energy Rev.* **96** 502–25